



**I  
N  
A  
O  
E**

# **Development of Methodologies for Characterization and Modeling of Devices for High Frequency Applications from Small-Signal S-parameters**

by  
**Germán Andrés Álvarez Botero**

A dissertation  
submitted to the Electronics Department  
in partial fulfillment of the requirements for the degree of

**D.Sc. in Electronics**

at the  
National Institute for Astrophysics, Optics and Electronics  
August, 2013  
Tonantzintla, Puebla

Advisors:

**Dr. Roberto Murphy Arteaga, INAOE**  
**Dr. Reydezel Torres Torres, INAOE**

©INAOE 2013

All rights reserved

The author hereby grants to INAOE permission to reproduce and to  
distribute copies of this thesis document in whole or in part



## Abstract

Due to the growing interest for using devices fabricated in BiCMOS technologies for microwave applications, the development of reliable models that represent the performance of heterojunction bipolar transistor (HBT) in high frequencies, is increasingly necessary in the design of integrated circuits. To contribute in this research area, this dissertation focuses on the development of models for high-frequency simulation both compact and equivalent circuit. These models allow not only to deepen the understanding of the physical phenomena emerging in advanced bipolar technologies, but also represent an important contribution to the evolution of the design assisted by circuit simulators, and the development of new microwave applications.

This dissertation is presented in a sequential way, from the study of the origin and physical interpretation of the losses associated with the required test structures for the measurement of small-signal parameters of HBTs. The resulting model that includes the parasitic effects introduced by the test structure shows that considering the effects emerging at high frequencies, such as the skin effect, a significant improvement is obtained in the de-embedding procedures. Thus, the development of this dissertation has contributed in improving the quality of de-embedding procedures, which directly affect the reliability of the measurement, characterization and modeling of BiCMOS devices.

Subsequently, the effects associated with the distributed nature of the HBTs were carefully analyzed, allowing the development of a hybrid model, i.e., a model resulting by combining equivalent circuit model and a compact model. The model proposed in this dissertation, together with its corres-

---

ponding parameter extraction methodology, allow to deepen in the understanding of the distributed effects that impact the electrical characteristics of an HBT's input and output. The results show an excellent simulation-experiment correlation up to 60 GHz, extending the frequency limits of current models used for the design of multi-stage ICs.

From the resulting hybrid models, once optimized, mentioned above, the impact on the power gain by not considering the appropriate characteristics of input and output is analyzed in this dissertation. This study was conducted for both common-emitter configuration as for common-base configuration. Finally, the analysis has been complemented by the development of an analytical expression that allows to set the limits where, comparatively, each transistor configuration has better features as a power amplifier, obtaining an excellent guide in the design of power amplifiers operating in the microwave range, field in which HBTs are widely used.

## Resumen

Debido al creciente interés de usar dispositivos fabricados en tecnologías BiCMOS para aplicaciones de microondas, el desarrollo de modelos confiables que representen el desempeño del transistor bipolar de heterounión (HBT, por sus siglas en inglés) en altas frecuencias, es cada día más necesario en el diseño de circuitos integrados. Para contribuir en este campo de investigación, esta disertación se enfoca en el desarrollo de modelos para la correspondiente simulación en altas frecuencias, tanto de forma compacta como de circuito equivalente. Estos modelos no sólo permiten profundizar en el entendimiento de los fenómenos físicos emergentes en tecnologías bipolares avanzadas, sino que además, presentan una importante contribución para la evolución del diseño asistido mediante simuladores de circuitos, y para el desarrollo de nuevas aplicaciones en el campo de las microondas.

La memoria escrita de esta tesis se presenta en forma secuencial, partiendo del estudio e interpretación física del origen de las pérdidas asociadas a las estructuras de prueba requeridas para la medición de los parámetros de pequeña señal de HBTs. El modelo resultante que incluye los efectos parásitos introducidos por dicha estructura de prueba ha mostrado que al considerar los efectos emergentes en altas frecuencias, como el efecto piel, se obtiene una mejora significativa en los procedimientos de des-incrustamiento. Así, con el desarrollo de esta disertación se contribuyó en el mejoramiento de la calidad de los procedimientos de des-incrustamiento, lo cual repercute directamente en la confiabilidad de los procesos de medición, caracterización y modelado de dispositivos BiCMOS.

Posteriormente, los efectos asociados a la naturaleza distribuida de los HBTs fueron analizados cuidadosamente, lo que permitió desarrollar un modelo híbrido, es decir, un modelo resultante al combinar un modelo de circuito equivalente y un modelo compacto. El modelo propuesto en esta disertación, en conjunto con su correspondiente metodología de extracción de parámetros, ha permitido profundizar en el entendimiento de los efectos que impactan las características eléctricas de entrada y salida del HBT en altas frecuencias. Los resultados muestran una excelente correlación simulación-experimento hasta 60 GHz, extendiendo los límites de frecuencia de los modelos actuales utilizados para el diseño de circuitos y contribuyendo significativamente en el diseño de circuitos integrados de múltiples etapas.

A partir de los modelos resultantes tras optimizar los modelos híbridos mencionados anteriormente, el impacto en la ganancia de potencia al no considerar las características adecuadas de entrada y salida es analizado en esta disertación. Éste estudio se desarrolló tanto para transistores configurados en emisor común, como para transistores configurados en base común. Finalmente, el presente análisis se ha complementado con el desarrollo de una expresión analítica, que permite establecer los límites donde comparativamente cada configuración del transistor presenta mejores características como amplificador de potencia, obteniendo una excelente guía para el diseño de amplificadores de este tipo operando en el rango de las microondas, campo en el cual los HBTs son ampliamente utilizados.

## Agradecimientos

Aprovecho estas líneas para expresar mi profunda gratitud a todas aquellas personas que durante mis estudios de doctorado me han brindado su apoyo, especialmente:

- Al Dr. Reydezel Torres, por confiar en mi para el desarrollo de este trabajo, por su permanente motivación, su inmensa colaboración y sus valiosas enseñanzas.
- Al Dr. Roberto Murphy, por la confianza, el apoyo y los valiosos aportes al desarrollo de esta tesis.
- A los investigadores, estudiantes y trabajadores del INAOE, por el ambiente propicio para la investigación en el que pude desarrollar este proyecto.
- Al CONACyT, por la beca otorgada que para la realización de mis estudios doctorales.
- Al IMEC, por los dispositivos que me fueron facilitados para el desarrollo de este trabajo.
- A mi madre, Fanny, por su apoyo incondicional y su voz de aliento en los momentos difíciles lejos de casa.
- A mi hermana, Claudia, y mis sobrinos, Juan Diego y Clara, por la motivación y apoyo que siempre me han brindado.
- A los amigos que me acompañaron momentos vividos durante este proceso.

- A Dios gracias.

# Contents

<b>Abstract</b>	<b>i</b>
<b>Resumen</b>	<b>iii</b>
<b>Agradecimientos</b>	<b>v</b>
<b>1 Introduction</b>	<b>1</b>
1.1 Modeling the HBT for Microwave Applications . . . . .	2
1.2 On-Wafer S-parameters Measurements . . . . .	4
1.3 Equivalent Circuit Modeling for Microwave HBTs . . . . .	6
1.4 Purpose and Outline of this Dissertation . . . . .	10
<b>2 Physical Modeling of Test Fixtures used for Probing Microwave BiCMOS Devices</b>	<b>12</b>
2.1 Generic Model for Shielded Test Structures . . . . .	13
2.1.1 Fabricated Prototypes . . . . .	16
2.2 Equivalent Circuit Modeling . . . . .	16
2.3 Model Verification . . . . .	20
2.4 Device Modeling Application . . . . .	23
2.5 Conclusions and Original Contributions . . . . .	25
<b>3 Modeling the Distributed Physical Effects in Microwave SiGe HBTs</b>	<b>26</b>



---

3.1	Modeling the Electrical Characteristics of the HBT's Output Port . . . . .	28
3.1.1	Proposed Model and Corresponding Extraction Methodology . . . . .	31
3.1.2	Model Verification . . . . .	34
3.2	Modeling the Electrical Characteristics in the HBT's Input . . . . .	35
3.2.1	Proposed Model and Corresponding Extraction Methodology . . . . .	36
3.2.2	Results and Discussion . . . . .	38
3.3	Conclusions and Original Contributions . . . . .	41
<b>4</b>	<b>Improving the Modeling for Power Amplification in CE and CB SiGe HBTs</b> . . . . .	<b>43</b>
4.1	Determination of the HBT's Substrate Parasitics . . . . .	44
4.2	Modeling the HBT in the Active Region . . . . .	47
4.3	Dependence of Power Gain on Base Impedance . . . . .	51
4.4	Conclusions and Original Contributions . . . . .	57
<b>5</b>	<b>General Conclusions</b> . . . . .	<b>58</b>
5.1	Test Fixtures for High-Frequency Characterization . . . . .	59
5.2	Parameter Extraction Methodologies . . . . .	59
5.3	Compact and Equivalent Circuit Models . . . . .	59
5.4	Emerging Modeling Topics . . . . .	60
<b>A</b>	<b>Publications Derived from this Dissertation</b> . . . . .	<b>61</b>
<b>B</b>	<b>Resumen Ejecutivo en Español</b> . . . . .	<b>66</b>

## Introduction

*"We have called it the Transistor, because it is a resistor or semiconductor device which can amplify electrical signals as they are transferred through it."*

Nobody could have foreseen the coming revolution when the invention of the transistor (*transfer-resistor*) was announced on June 30, 1948, with this words [1]. However, today it is hard to imagine any device more important to modern electronics than the transistor [2]; it is part of calculators, telephones, computers, automobiles, radios, televisions, kitchen appliances, clothing, jewelry, toys, medical implants and thousands of other electronic apparatuses.



**Figure 1.1:** A replica of the first working transistor, AT&T labs, 1948.

Modern transistors used for these applications work on the same basic principles as the original bipolar junction transistor (Fig 1 [1]), created by Bardeen, Brattain, and Shockley in the late 40's [3], namely: (1) minority-carrier injection into the base layer, which increases exponen-

tially with forward emitter bias; (2) application of reverse voltage at the collector junction; (3) favorable geometry and doping levels so as to obtain good emitter-to-collector efficiency [4]. In fact, these fundamental conceptual similarities between the earliest junction transistors and modern bipolar transistors contributed to many of the theoretical models originally formulated, and continue to apply to new devices despite the rapid technological advancements that have occurred over the years. For instance, the diffusion theory for minority carriers, originally presented by Shockley [5], has continued providing the basis for modeling minority-carrier base transport for almost five decades, without considering that this interpretation assumes "large" device dimensions, that is, dimensions much greater than a mean-free path length, and therefore, for sub-micrometric devices (where the dimensions are now comparable to a mean-free path for scattering), these classical descriptions must be carefully reconsidered and updated. Additionally, owing to the advent of wireless communications, integrated bipolar circuit techniques have found wide-spread use in radio frequency (RF) applications [6], increasing the complexity of bipolar processes, and making device modeling with the goal to reliably predict the behavior of integrated circuits by means of computer simulations of vital importance.

## 1.1 Modeling the HBT for Microwave Applications

Given that the first bipolar transistor was built from germanium (Ge) [7, 8], the concept of heterojunction bipolar transistor (HBT) is surprisingly old, dating in fact to the first transistor patent. It seems clear that Shockley et al. envisioned the combination of Si (wide bandgap emitter) and Ge (narrow bandgap base) to form a SiGe HBT; however, only after four decades of progress in epitaxial deposition techniques, it has been possible to form thin base layers of strained SiGe on silicon substrates, incorporating HBTs to silicon IC technology.

SiGe HBTs appear in virtually every IC used in the high frequency analog market segments. SiGe devices are used in both handsets and base stations for CDMA and GSM standards at 900MHz and 2.4 GHz; in wireless local area networks (WLAN) chipsets at 2.4 GHz; in high-speed/high-capacity net-

work applications such as synchronous optical network (SONET) transmit and receive modules (40 Gb/s, 100 Gb/s Ethernet and beyond); in automotive radar (77 GHz), as well as in emerging applications up to 170 GHz for industrial, medical, security, space, radio-astronomy, and other applications that include discrete devices and products with lower levels of integration such as LNAs, VCOs, mixers, power amplifiers (PA) and GPS receivers [9].

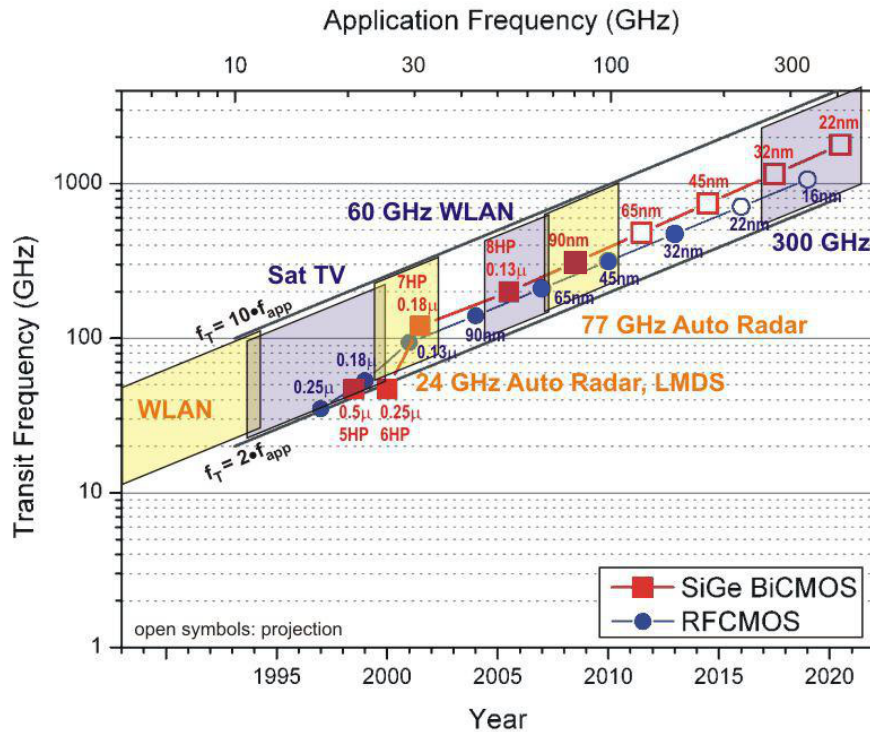


**Figure 1.2:** RF application spectrum overlaid with technology performance [10].

A mapping for technologies showing the RF application frequency spectrum for RFCMOS and SiGe BiCMOS is illustrated in Fig. 1.2. This figure clearly indicates that RF BiCMOS technologies have been continuously enhanced. Unfortunately, computer-aided-design (CAD) capabilities have not been able to follow the rapid process evolution. Thus, improved models such as HICUM [11] and MEXTRAM [12], that include new effects from high-speed bipolar technologies, have inadequately been used for modern RF

circuit design. Moreover, since the number of parameters associated with these models has increased considerably, they are becoming more complicated and less manageable. Therefore, a popular and reliable alternative to model the bipolar transistors at high frequency is using equivalent circuit models [13–15], which generally are developed from scattering parameter (S-parameter) measurements. These important small-signal network parameters are explained in the following section.

## 1.2 On-Wafer S-parameters Measurements

In order to completely characterize an unknown device, usually referred to as Device Under Test (DUT), it is a common practice to make measurements at various conditions and compute a set of parameters. These parameters can be used to completely describe the electrical behavior of the device when considered as a linear network. For high frequency characterization, S-parameters are determined by measuring the magnitude and phase of reflected, and transmitted signals when a power wave swept in frequency is applied to the device input (or output) terminal while the output (or input) terminal presents the reference impedance of the measuring equipment [16]. In the case of a simple

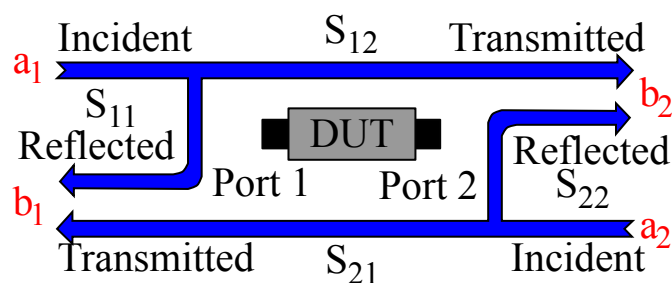


**Figure 1.3:** DUT configured as a two-port network showing the S-parameter definitions.

two-port network, such as the one illustrated in Fig. 1.3,  $S_{11}$  is equivalent to the complex reflection coefficient at the input of the DUT, while  $S_{21}$  is the forward complex transmission coefficient. Likewise, by placing the source at the output port of the DUT and terminating the input port at the reference impedance of the system, it is possible to measure the other two (reverse)

S-parameters. In the latter case,  $S_{22}$  is the complex reflection coefficient at the output of the DUT, whereas  $S_{12}$  is the reverse complex transmission coefficient.

In the case illustrated in Fig. 1.3, the DUT can be described by a  $2 \times 2$  matrix. Typically, the most popular matrices to analyze a two-port network are in terms of the Z, Y, ABCD or even H-parameters. However, S-parameters are measured instead due to the impossibility of directly obtaining the conventional network parameters at high frequencies [17]. According to Fig. 1.3, the S-parameter matrix can be defined as:

$$\begin{bmatrix} b_1 \\ b_2 \end{bmatrix} = \begin{bmatrix} S_{11} & S_{12} \\ S_{21} & S_{22} \end{bmatrix} \begin{bmatrix} a_1 \\ a_2 \end{bmatrix} \quad (1.1)$$

where  $a_1$  and  $a_2$  are the incident waves, and  $b_1$  and  $b_2$  are the reflected waves at the input and output ports. Thus, once S-parameters have been measured, the matrix defined by equation 1.1 can be converted to the equivalent Z, Y, or H matrix to perform the proper analysis of the two-port network in terms of the input and output voltages and currents [17].

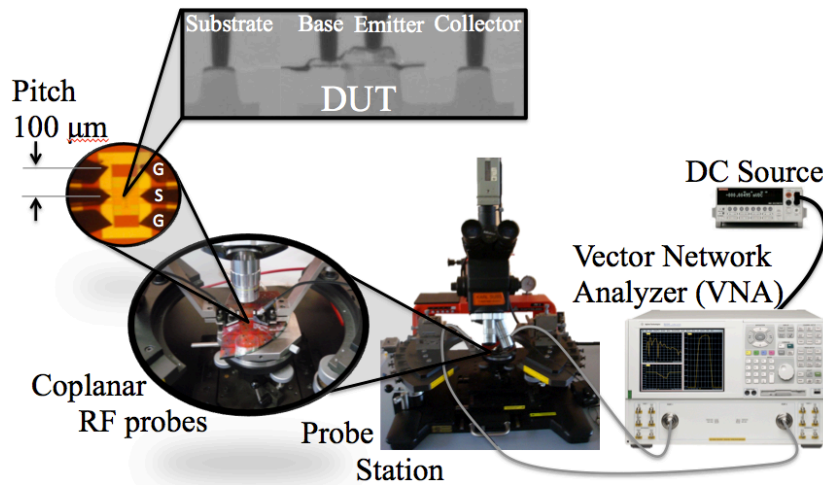


*Figure 1.4: Measurement setup for on-wafer S-parameters.*

The RF test system used to obtain the experimental data from the different devices studied throughout this research project, is composed of an

Agilent E8361A vector network analyzer (VNA), connected through RF cables to ground-signal-ground (G-S-G) coplanar probes with a  $100\ \mu\text{m}$  of pitch; it is illustrated in Fig 1.4. In cases where a DC bias were required, an external power source can be connected through a bias-T connection incorporated within the VNA, biasing the DUT simultaneously as RF signals are applied and measured.

In all the studied cases in this dissertation, the equipment was previously calibrated up to the probe tips, as shown in Fig. 1.5, Using an off-wafer LRM (line-reflect-match) procedure, and an impedance-standard-substrate, establishing a reference impedance of  $50\ \Omega$ . Additionally, the measurements used throughout this thesis, were performed applying a power of  $-20\ \text{dBm}$  at each port to maintain the DUTs within small-signal operation conditions. More details about the measurement setup, RF test fixtures, and experimental data processing are given later in this dissertation.

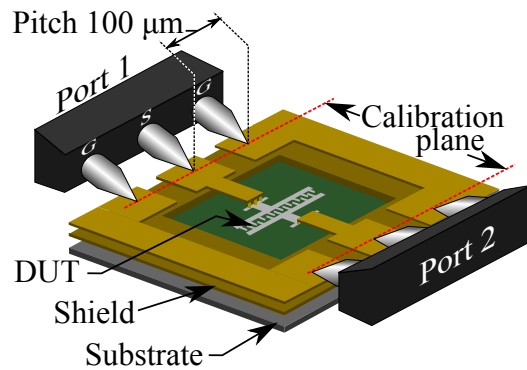


*Figure 1.5: Test structure for performing S-parameter measurements showing the pad configuration for probing.*

### 1.3 Equivalent Circuit Modeling for Microwave HBTs

Although there are different ways to predict the transistor's response to a certain stimulus, not all of them are appropriate to perform simulations for IC design purposes. Thus, in spite of the excellent results obtained when solving the fundamental semiconductor equations throughout the device's 3D structure, this approach is not efficient to be used on IC simulations since the calculations take very long time, restricting its application to single device analysis. Therefore, equivalent circuit models and compact models are used



to make computing time-effective IC simulations. In this case, important demands for a good RF simulation can be fulfilled, such as:

- *Bias dependence consideration:* HBTs consist essentially of two  $pn$  diodes that share a thin  $p$  region: the base of the transistor. Thus, four operation conditions exist:
  1. Off state, with both  $pn$  junctions reversely biased and zero current flowing.
  2. Saturation, with both  $pn$  junctions in forward bias; therefore, the HBT acts approximately as a short circuit, and current flow is limited by the extrinsic resistances.
  3. Active-forward operation, with the base-emitter junction in forward bias, and the base-collector junction in reverse bias. In this operation condition, the base-emitter current  $i_b$  controls the emitter-collector current  $i_c$ , since the majority of the electrons leaving the emitter diffuse through the base into the collector, thereby contributing to  $i_c$ ; only a small fraction recombines in the base, yielding  $i_b$ .
  4. Reverse operation, which is similar to active-forward operation, but with the collector and emitter interchanged.

It is important to remark at this point that usually the epitaxial layer structure of the HBT is optimized in a way to improve forward-active operation, while the reverse operation will provide poor results. Therefore, a model obtained in a certain configuration of terminals, for instance common-emitter, will not be useful in other (for instance common-base), as a consequence that the *HBTs are not symmetrical devices*.

- *Scalability considerations:* The input and output matching on the HBT depends on its size [18]. Additionally, in RF-IC design many transistors with different layouts and dimensions are used. Consequently, a model must be adequate to represent the electrical characteristics of a device as a function of its geometry.
- *Accuracy within the GHz range:* HBTs have a very large cut-off frequency ( $f_T$ , the frequency of unity short-circuit current gain) and



$f_{max}$  (the maximum frequency at which power gain occurs), however, these important figures of merit are limited by the interaction of many high frequency effects, that must be adequately incorporated in the modeling in order to determine the properties limitations of the device.

Although an ideal HBT RF-model should be scalable and accurate for any bias condition within the GHz range, it is very difficult to reach that goal. However, by means of the equivalent circuit modeling, it is possible to achieve a very good representation of the electrical behavior of the transistor at high frequencies owing to its clear correlation with the device's topology. Besides, equivalent circuits present a simple implementation and evaluation in traditional circuit simulators such as SPICE.

In an equivalent circuit model, each effect influencing the HBT's behavior is represented by means of lumped elements that can be extracted directly or indirectly from I-V, C-V, or S-parameter measurements. However, since many times these models are completely based in the interpretation of experimental data, the proposed topology for its analysis is very important. In this regard, the small-signal behavior is usually described by two topologies: T and  $\pi$  equivalent circuits.

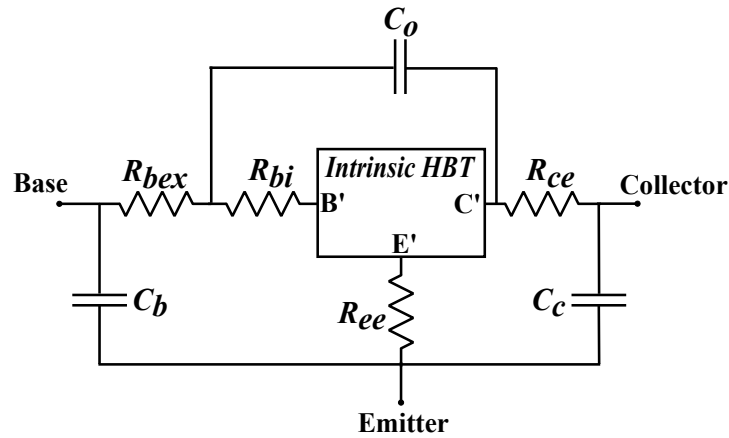


**Figure 1.6:** Small-signal model of an HBT illustrating its extrinsic elements.

Fig 1.6 shows a schematic of a small-signal HBT equivalent circuit, which can be divided in two groups of elements: *i*) *extrinsic elements*, that could be

dependent or not on the applied bias, and usually are considered as parasitics in the transistor operation; *ii*) *intrinsic elements*, that represent the HBT operation in the active region. The intrinsic block in Fig 1.6 is commonly modeled by means of  $\pi - g_m$ ,  $\pi - \beta$ , or T- $\alpha$  topologies, which are shown in Figs 1.7 (a), (b) and (c) respectively.

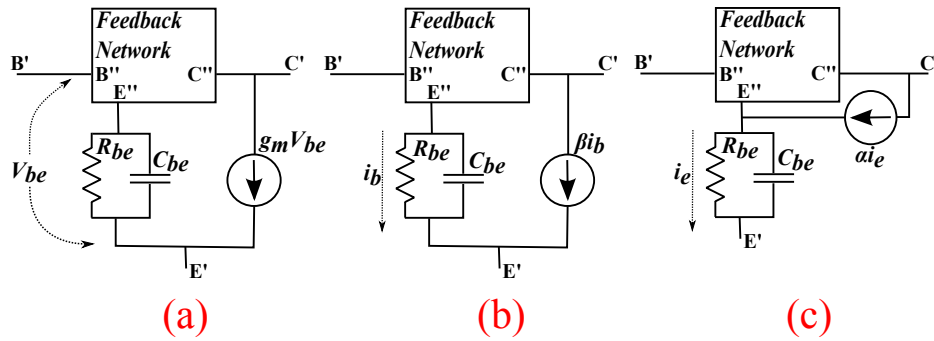


Figure 1.7: Intrinsic topologies (a)  $\pi - g_m$ , (b)  $\pi - \beta$  and (c) T- $\alpha$  of an HBT.

Each one of the preceding intrinsic topologies in turn is constituted by a feedback network, which is related to the device physics, and its complexity level is related to the accuracy of the model. Two of the most common feedback circuits found in the literature are illustrated in Fig 1.8, obtaining in this case six basic intrinsic circuit topologies.

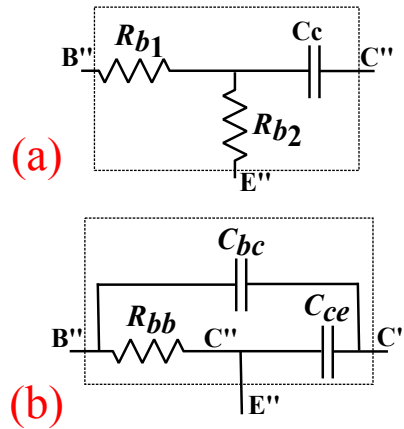


Figure 1.8: Simple feedback networks that would be used together with  $\pi - g_m$ ,  $\pi - \beta$  or T- $\alpha$  topologies.

In order to relate these different intrinsic equivalent circuits, it is possible to use expressions such as  $\beta = g_m R_{be}$ , that relate the topologies  $\pi - g_m$  and  $\pi - \beta$  [19]. In a similar way, the expressions that relate the T- $\alpha$  and  $\pi - g_m$  topologies were

developed by Teeter *et al.* [20].

For bipolar transistors, both T and  $\pi$  topologies are in use. In general, the T-topology is pretty clear correlating the device physical structure with its equivalent circuit model, whereas the  $\pi$  topology has a more intuitive link to device electrical behavior; hence, it gives a better vision for IC design [20, 21]. Therefore, both topologies should be valid to describe the electrical behavior of an HBT at high frequencies; however, they are not equivalent in all cases, depending, for instance, on the transit time, which in turn is strongly dependent on the non-linear effects occurring on the base region.

Thus, due to the difficulty in obtaining easy-to-use models for their application on standard simulation tools, many designers of RF circuits are still using inadequate models for representing the HBT. Sometimes, exact RF models may involve very complicated formulations, making their implementation difficult, whereas simple models may yield inaccurate results. Hence, a compromise between complexity and accuracy must be established in order to develop feasible models for RF applications.

## 1.4 Purpose and Outline of this Dissertation

This dissertation focuses on equivalent circuit and compact models for the high-frequency characteristics of modern heterojunction bipolar transistors. Classical descriptions of the high-frequency behavior are reexamined, leading to a set of well-founded small-signal models, that describe the high-frequency operation of state-of-the-art devices more soundly, obtaining therefore an original, novel and substantial contribution to the modeling of SiGe BiCMOS devices at microwave frequencies.

The main topic of this dissertation is addressed starting, in *Chapter 2*, by developing improved models for the test fixtures used for probing HBTs at microwave frequencies, in order to understand and include the high frequency physical effects in the deembedding procedures. Once that the experimental data have been deembedded reliably, new parameter extraction strategies and procedures are proposed in order to perform transistor modeling, and the distributed effects of the HBT are analyzed in *Chapter 3*. In *Chapter 4*, the impact of these effects is studied according to the configuration used

---

for the transistor. Finally, the conclusions derived from this dissertation are summarized in *Chapter 5*.

## Physical Modeling of Test Fixtures used for Probing Microwave BiCMOS Devices

THE characterization and modeling of microwave devices require high-frequency on-wafer measurements [22, 23]. In this case, to make a connection with the probe tips and to apply the RF stimulus to the device under test (DUT), a test fixture is necessary. This introduces considerable parasitic effects between the calibrated reference plane and the DUT, which are generally removed from the experimental data using a de-embedding procedure not necessarily considering their physical origin [24]. As devices are scaled down and the operating frequency ( $f$ ) rises, however, the impact of the test fixtures on the RF measurements is increased and further analysis of these structures is mandatory [25]. Moreover, de-embedding these effects might not be enough for certain cases [26]. In fact, a more complete knowledge of the influence of the test fixtures is needed to define the frequency range up to where the test fixture is practical, to optimize the layout design of the pads, and to evaluate the sensitivity of specific DUT model parameters to a particular de-embedding method.

The importance of characterizing and modeling test fixtures for developing appropriate de-embedding procedures relies on the fact that the characterization of high-performance transistors from S-parameter measurements allows the appropriate assessment of the corresponding performance [27]. In this regard, an area of particular concern and interest to device modelers and circuit designers is the improvement of the S-parameter measurement metho-

dology as the measurement frequency extends to microwaves and beyond.

Approaches such as modeling the probe pads, interconnections, and the DUT in a cascade configuration have been proposed, and these aim at identifying and removing the parasitic effects from raw measurements [28]. However, understanding the origin of the parasitics as well as their relation to the embedding network layout is not possible using these techniques. The relation with the physical structure is more evident when the unwanted effects of the test fixtures are modeled separating their influence in admittance and impedance blocks [25, 29–31], a methodology which in turn has allowed for a deeper understanding of these high frequency effects through the development of equivalent circuit models [25, 26, 32].

Nevertheless, most of these models consist of frequency independent circuit elements, and the modeling of crucial high frequency effects, such as the skin effect, which significantly affects the series resistive and inductive elements in the models for on-wafer pad structures, tend to produce very large circuits [33], increasing the complexity of the extraction methodologies. Therefore, in order to obtain a more reliable set of de-embedded data, special attention is necessary. Thus, throughout this chapter, a simple extraction methodology based on fundamental microwave engineering is proposed in order to incorporate the skin effect into a compact model for a test fixture. The developed model is then used to de-embed the HBTs, which are the main object of study in this work..

## 2.1 Generic Model for Shielded Test Structures

The most popular coplanar probe configuration to measure single-ended on-wafer S-parameters is G-S-G [34]. Its principal advantage is the good confinement of the electric field around the signal probe [35]. Thus, the electric field from the signal (S) pad terminates on the ground (G) pads on either side, as illustrated on Fig. 2.1(a). As can be seen in this figure, in a conventional test structure to probe a DUT with a G-S-G pads, the pads are formed in the first metal level (the closest to the substrate), yielding an undesired coupling between the signal and the ground pads through the substrate. Hence, a parasitic capacitance appears due to the distribution of the electric field lines in the pad corners, and a lossy network is introduced.

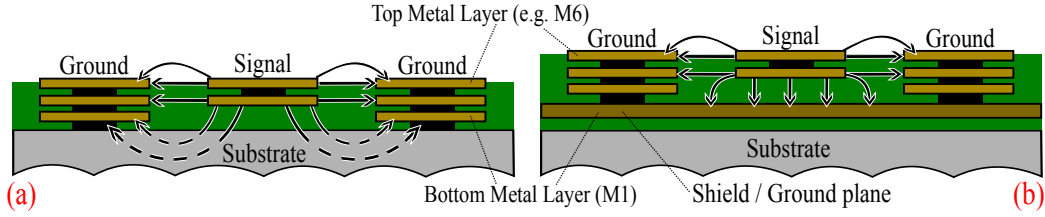


**Figure 2.1:** Cross sectional view showing the distribution of the electric field in: through the substrate (a) a conventional test fixture and, (b) a shielded test fixture.

Thus, to prevent the coupling of the signal and ground pads, it is a common practice to shield the pads from the substrate using a solid metal ground plane extending in every direction under the signal pad [36]. Therefore, the electric field is confined between the ground plane and the probe pads, as shown in Fig. 2.1(b).

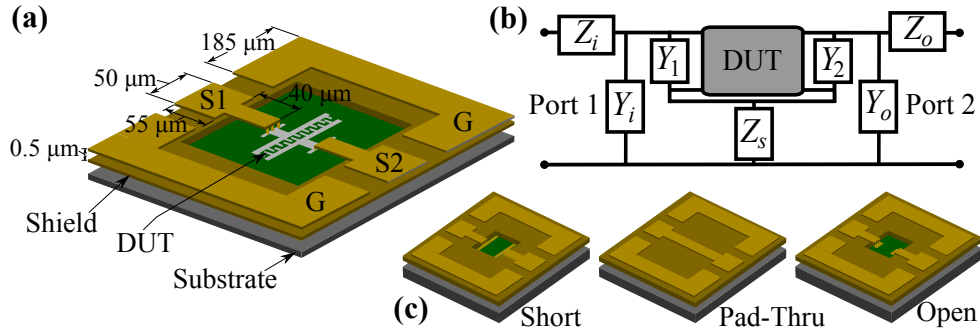


**Figure 2.2:** (a) Sketch of a DUT embedded in a test fixture, (b) corresponding equivalent circuit model consisting of generic impedance and admittance blocks, and (c) associated dummy structures for de-embedding.

As can be seen in Fig. 2.2(a), a window at the center of the shield is designed to interconnect the pads with the DUT. In this case, the test structure including the DUT can be represented by the circuit shown in Fig. 2.2(b), which considers the corresponding parasitic effects using generic impedance and admittance blocks. In this case,  $Z_i$  and  $Z_o$  include the series parasitics associated with the pads and the lines interconnecting the test fixture with the DUT,  $Y_i$  and  $Y_o$  take into account the electrical coupling from the signal pads to the ground pads and the shielding plane,  $Y_1$  and  $Y_2$  are used to represent the shunt parasitics occurring at the test-fixture-to-DUT interface,

and finally  $Z_S$  is associated with the interconnections between the DUT and the ground pads.

At this point, it is important to clarify that before developing a model based on *RLGC* parameters [16] for the test fixture, the admittances and impedances in the model of Fig. 2.2(b) have to be determined as a function of frequency. For this purpose, additional structures (i.e., dummy structures) are used. These structures are shown in Fig. 2.2(c), whereas the corresponding equivalent circuits are shown in Fig. 2.3.

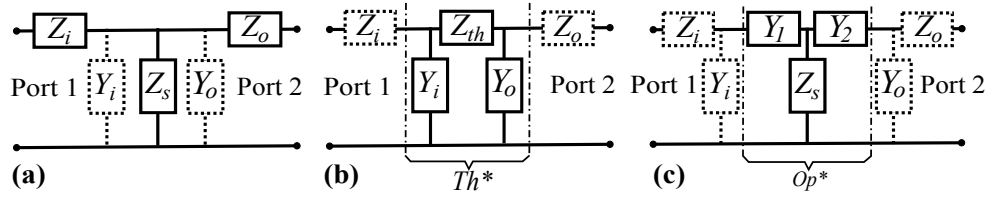


Figure 2.3: Equivalent circuit models for the dummy structures.

Firstly, the series elements  $Z_i$ ,  $Z_o$ , and  $Z_s$  are obtained from measurements performed to the Short structure. Notice in Fig. 2.3 that  $1/Y_i \gg Z_s$  and  $1/Y_o \gg Z_s$  were assumed; therefore, in this case:

$$Z_i = Z_{11_{Sh}} - Z_{12_{Sh}} \quad (2.1)$$

$$Z_o = Z_{22_{Sh}} - Z_{12_{Sh}} \quad (2.2)$$

$$Z_s = Z_{12_{Sh}} \quad (2.3)$$

where the S-parameters associated with the Short structure were converted to Z-parameters and present the subscript *Sh*.

Once the series impedances (i.e.,  $Z_i$  and  $Z_o$ ) have been determined, their effect can be removed from the experimental S-parameters corresponding to the Pad-Through structure using simple two-port network parameter transformations. The resulting parameters are subscripted with  $Th^*$  and can be related to the model in solid lines in Fig. 2.3(b); thus,  $Y_i$  and  $Y_o$  can be obtained from the  $Y_{Th^*}$ -parameters using:

$$Y_i = Y_{11_{Th^*}} + Y_{12_{Th^*}} \quad (2.4)$$

$$Y_o = Y_{22_{Th^*}} + Y_{21_{Th^*}} \quad (2.5)$$



where  $Y_{12_{Th^*}} = Y_{21_{Th^*}} = 1/Z_{th}$  can be obtained directly from the experimental data. Thus, notice in Fig. 2.3(b) that  $Z_{th}$  represents the line interconnecting the port-1 with the port-2 signal pads and its calculation is not necessary within the present analysis.

Afterwards,  $Z_i$ ,  $Z_o$ ,  $Y_i$  and  $Y_o$ , are removed from the S-parameters associated with the Open structure, yielding the model shown in solid lines in Fig. 2.3(c). Thus, from the corresponding Z-parameters,  $Y_1$  and  $Y_2$  can be determined as

$$Y_1 = [Z_{11_{Op^*}} - Z_s]^{-1} \quad (2.6)$$

$$Y_2 = [Z_{22_{Op^*}} - Z_s]^{-1} \quad (2.7)$$

where the subscript  $Op^*$  is used to denote the Z-parameters of the model in solid lines in Fig. 2.3(c).

Once all the elements in the model shown in Fig. 2.2(b) are determined, *RLGC* parameters can be used to represent the variation of these impedances and admittances as a function of frequency. This is explained hereafter.

### 2.1.1 Fabricated Prototypes

Before developing the equivalent circuit models for the test fixture, the structures shown in Fig. 2.3 were fabricated on a  $0.13\mu\text{m}$  BiCMOS process. All these structures present a ground shield implemented in the bottom metal layer available in the process (i.e., level-1 metal), which is connected to the ground pads of the test fixture to correctly establish the ground reference. These pads, as well as those for the signals at port-1 and port-2, are made of aluminum at the top metal level. Furthermore, the pads are configured for using G-S-G coplanar RF probes with a pitch of  $100\mu\text{m}$  as illustrated in Fig. 1.5. The procedure to perform the S-parameter measurements up to  $f = 60$  GHz is the same described in section 1.2.

## 2.2 Equivalent Circuit Modeling

The methodology proposed here to obtain the equivalent circuit representation for the series and shunt parasitics is illustrated for the case of  $Z_s$  and the

blocks at the left of the DUT (i.e., at port-1 in Fig. 2.2(b)), since the parameters associated to port-2 can be obtained in a similar way by applying the same methodology using the corresponding experimental data. Before starting explaining the equivalent circuit for the test structure, it is important to remark the fact that for the maximum frequency analyzed in this work (i.e., 60 GHz) the corresponding wavelength is approximately 4.9 mm, which is very large in comparison to the maximum length occurring in the structure (approximately 90  $\mu\text{m}$ ). This allows us to neglect the distributed nature of the pad, which is observed at much higher frequencies, and a lumped circuit such as that shown in Fig. 2.4 results adequate.

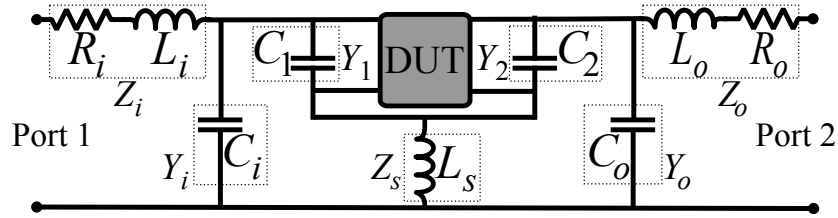


**Figure 2.4:** Equivalent circuit model for the test fixture using RLGC elements.

In Fig. 2.2(b),  $Z_i$  includes the series effects of the pads and lines used to reach the DUT. These effects are related to the finite resistivity of the metal used to form the pads and the inductance associated with the current loop formed by the signal pads and the return path. Therefore,  $Z_i$  can be modeled as shown in Fig. 2.4 by using an equivalent resistance and inductance  $R_i$  and  $L_i$ , respectively. The value of these parameters depends on material and geometrical factors, but it is important to take into account that  $R_i$  and  $L_i$  are also strongly dependent on  $f$  due to the confinement of the current in the surface of a metal due to the skin effect, which is noticeable within the gigahertz range. This effect is neglected in previous approaches for modeling RF probing pads, either limiting the frequency range of validity of the model [37], or requiring the use of multiple resistances and inductances [33].

Two equations that accurately represent the  $f$ -dependent  $R_i$  and  $L_i$ , including the skin effect are [38]:

$$R_i = R_{LFi} + K_i \sqrt{f} \quad (2.8)$$

$$L_i = L_{HF i} + \frac{K_i}{2\pi\sqrt{f}} \quad (2.9)$$

where  $R_{LFi}$ ,  $L_{HF_i}$  and  $K_i$  are independent of  $f$ . Thus, considering equations (2.8), (2.9) and  $Z_i = R_i + j2\pi f L_i$ ,  $R_{LFi}$  and  $K_i$  can be determined by performing a linear regression of the experimental  $\text{Re}(Z_i)$  versus  $\sqrt{f}$  data, whereas  $L_{HF_i}$  can be obtained from the slope of a linear regression of the  $2\pi\sqrt{f} \text{Im}(Z_i)$  versus  $2\pi\sqrt{f}$  data. The extraction of these parameters is shown in Fig. 2.5(a) and (b) for  $f > 15$  GHz. Observe that  $K_i$ , extracted in Fig. 2.5, can be consistently obtained using a regression based either on (2.8) or (2.9); this is due to the fact that  $K_i$  accounts for the reduction of the cross-sectional area where the current is flowing through the pads (i.e., the skin effect), which impacts both  $R_i$  and  $L_i$  equally.

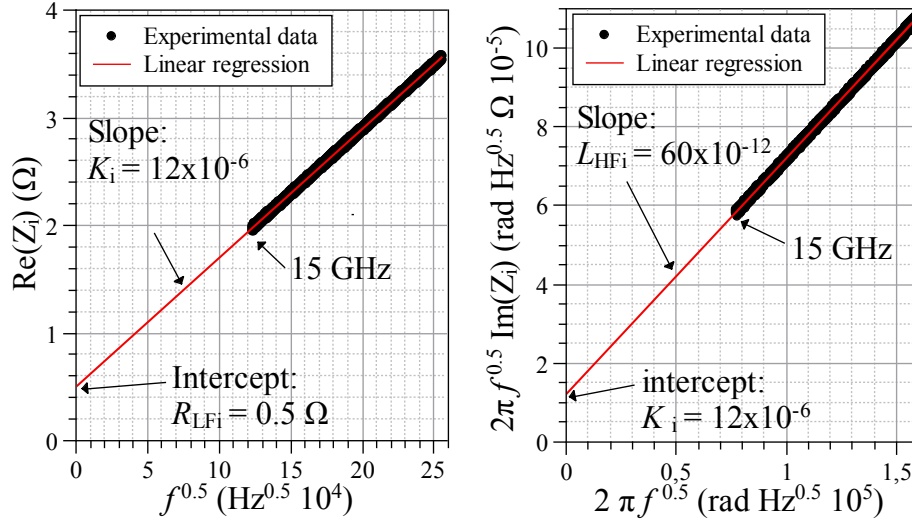
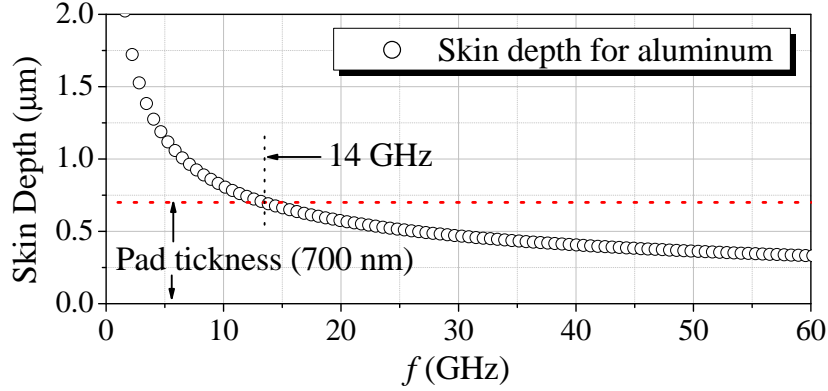


Figure 2.5: Linear regressions used to determine  $R_{LFi}$ ,  $K_i$ , and  $L_{HF_i}$ .

At this point, it is important to remark that the parameters extracted in Fig. 2.5(a) and (b), were considered for  $f > 15$  GHz, since the frequency dependent nature of  $|Z_i|$  is only observed beyond the frequency at which the skin depth is as small as the pad thickness. For the case of the studied pads, made of aluminum, this occurs approximately at  $f = 14$  GHz, since at this frequency  $\delta \approx 700$  nm (i.e. the metal pad thickness), as is shown in Fig. 2.6.



**Figure 2.6:** Skin depth calculated for aluminum, which is the metal used to form the probing pads used in this project.

It is convenient also to mention that  $Z_i$  and  $Z_o$  are associated with the series parasitics occurring at the input and output ports, including the corresponding signal and ground paths. However, part of the series parasitics are presented at both ports; for instance, those related to the thin vias used to interconnect the DUT reference terminal to ground. This effect is represented by means of  $Z_s$ , which can be modeled by means of an inductance ( $L_s$ ). In contrast to  $L_i$  and  $L_o$ ,  $L_s$  can be considered as independent of  $f$  due to the relatively small size of the vias used as vertical interconnects; thus, the impact of skin effect is not important for  $Z_s$  at the frequencies of interest in this work. Hence, assuming  $Z_s \approx j2\pi fL_s$ ,  $L_s$  is directly obtained from the slope of the  $\text{Im}(Z_s)/2\pi$  versus  $f$  curve. The determination of this parameter is shown in Fig. 2.7(a).

The shunt admittances,  $Y_i$  and  $Y_o$  include the capacitive effect occurring between the signal pad and the return path formed by the ground pads and the ground shield. In practice, the associated capacitors present losses due to the finite value of the loss tangent of the field oxide. For  $f$  up to some tens of gigahertz, however, the impact of these losses on  $Y_i$  is small and a single capacitance ( $C_i$ ) can be used to represent the shunt admittance. Moreover,  $C_i$  presents an approximately constant value with  $f$  as long as the silicon substrate effects are negligible. So,  $C_i$  can be easily determined from a regression of the  $\text{Im}(Y_i)/2\pi$  versus  $f$  curve, as shown in Fig 2.7(b).

Finally, the admittances  $Y_1$  and  $Y_2$  are associated with small capacitances at the test-fixture-to-DUT transition. For the case of  $Y_1$ , a capacitance  $C_1$  is used to represent this effect and can be determined from the slope of a linear regression of the  $\text{Im}(Y_1)/2\pi$  versus  $f$  experimental data, as shown in Fig. 2.7(c).

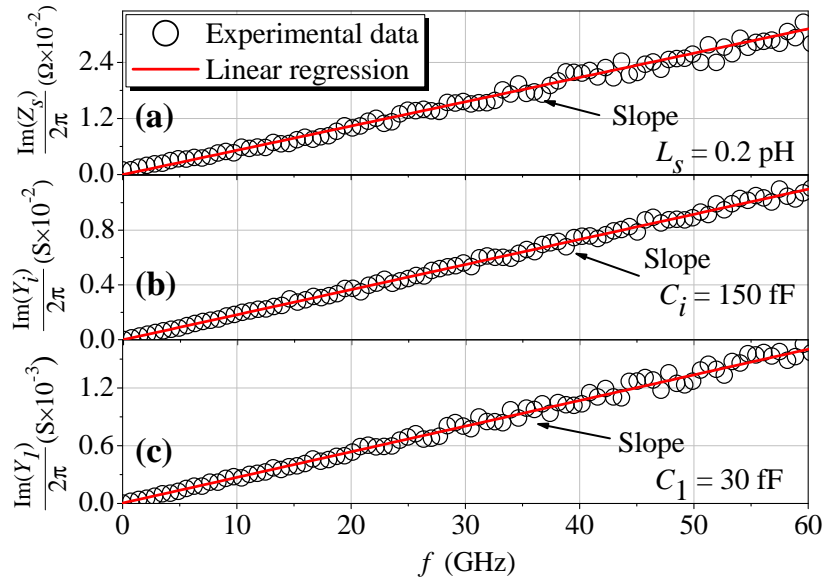
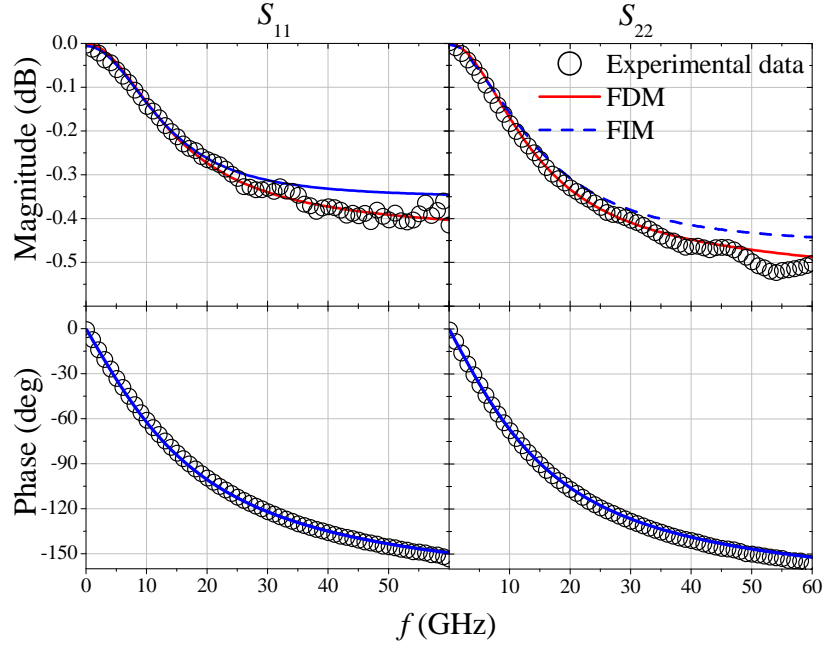


Figure 2.7: Linear regressions used to determine (a)  $L_s$ , (b)  $C_i$ , and (c)  $C_1$ .

## 2.3 Model Verification

In order to point out the advantages of using the proposed model and parameter extraction methodology, the model in Fig. 4 was implemented in Agilent's ADS circuit simulator for two cases: using  $f$ -independent series elements (the corresponding model is referred to as FIM), and using (2.8) and (2.9) to represent the  $f$  dependent nature of the series resistances and inductances of the structure (FDM model). Then, a comparison involving  $S_{11}$  and  $S_{22}$  was performed since  $S_{12}$  and  $S_{21}$  present a magnitude below  $-30$  dB within the measured  $f$ -range due to the excellent isolation between ports in the fabricated test fixture. It is important to point out the fact that even though many circuit simulators are readily available to include frequency

dependent elements, this type of effect can also be directly implemented in SPICE using arrays of frequency independent elements [39].



**Figure 2.8:** Comparison between simulated and experimental data corresponding to the Open structure when using the models that consider  $f$ -independent (FIM) and  $f$ -dependent (FDM) series elements.

As shown in Fig. 2.8, the two studied models acceptably reproduce the experimental  $S_{11}$  and  $S_{22}$  measured data from the Open structure within the whole analyzed  $f$ -range. The relatively good model-experiment correlation obtained when using FIM is due to the fact that the shunt elements are dominant for the Open structure, and their impact on the  $f$ -dependent series elements on the measured S-parameters is small.

On the other hand, the dominant effects in the Short structure are those associated with the series elements, which are  $f$ -dependent. Thus, notice in Fig. 2.9 that FIM fails to represent the experimental  $S_{11}$  and  $S_{22}$  data for  $f > 30$  GHz. In fact, beyond this frequency,  $R_i$  and  $R_o$  substantially differ from their corresponding values at low frequencies (i.e.,  $R_{LFi}$  and  $R_{LFO}$ , respectively) and considering their  $f$ -dependent nature becomes mandatory

to obtain realistic simulation results. In this regard, extracting the associated parameters using the proposed methodology yields excellent results at least up to  $f=60$  GHz, as shown in Fig. 2.9.

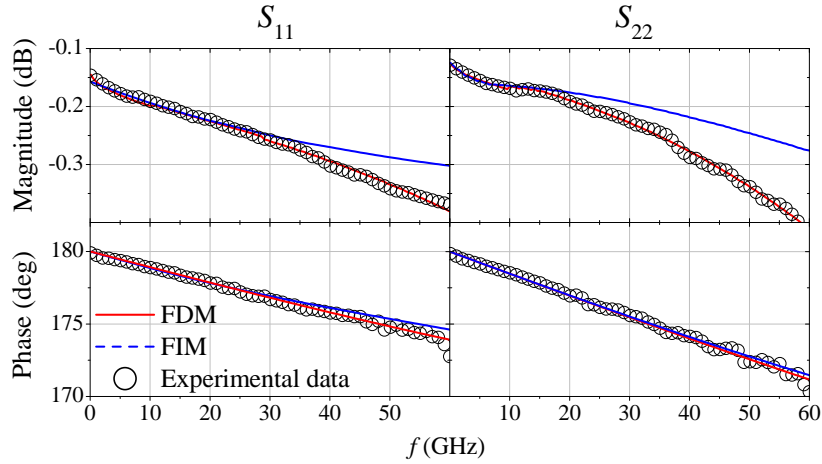


**Figure 2.9:** Comparison between simulated and experimental data corresponding to the Short structure when using the models that consider  $f$ -independent (FIM) and  $f$ -dependent (FDM) series elements.

Notice also in Figs. 2.8 and 2.9 that the experimental data corresponding to the dummy structures includes considerable noise beyond 30 GHz, which is inherent to reflective structures fabricated in BiCMOS processes. In consequence, these noisy data may introduce errors when applying the de-embedding procedure. For this reason, when an appropriate representation of the dummy structure is achieved using equivalent circuit models, these models can be used instead of directly using the noisy data corresponding to the dummy structure; this allows to reduce the noise observed in the final de-embedded data.

In Table 2.1 the extracted parameters are summarized, which allow to compare the obtained values for the FIM and FDM models using the proposed methodology.

Parameter	FIM	FDM
$R_i$ ( $\Omega$ )	0.62	$0.5 + 12 \times 10^{-6} \sqrt{f}$
$L_i$ (pH)	7.3	$6 + \frac{1.2 \times 10^{-6}}{2\pi\sqrt{f}}$
$C_i$ (fF)	146	150
$C_1$ (fF)	33	30
$L_s$ (pH)	0.5	0.2
$C_2$ (fF)	35	31
$C_o$ (pF)	170	159
$L_o$ (pH)	7.4	$6.9 + \frac{1.3 \times 10^{-6}}{2\pi\sqrt{f}}$
$R_o$ ( $\Omega$ )	0.48	$0.4 + 1.3 \times 10^{-6} \sqrt{f}$

*Table 2.1: Extracted parameters.*

## 2.4 Device Modeling Application

In order to verify the usefulness of the proposed model and extraction methodology, the models discussed in section 2.3 are used here to de-embed measurements of a common emitter/substrate HBT fabricated on a p-type Si substrate. This device presents a total width  $W_e = 1 \mu\text{m}$ , emitter length  $L_e = 0.13 \mu\text{m}$ , and was biased at  $V_{be} = 0.8 \text{ V}$  and  $V_{ce} = 1.2 \text{ V}$  in order to observe the potential modeling errors when the device is operated in the active region.

At this point, it is important to mention that the measurements of the DUT, including the effect of the test fixture are referred to as raw measurements. Thus, once these raw measurements are performed, a de-embedding method is applied to remove the effect of the test fixture using generic impedance and admittance blocks [25]. This is the most common way to perform a de-embedding, and even though no physical significance is associated to the generic blocks, the corresponding results can be considered as accurate [25]. Subsequently, the raw measurements are de-embedded again, but now using the FIM and FDM to represent the effect of the test fixture; the results are compared in Fig. 2.10. Notice the better model-experiment correlation when FDM is used, pointing out the importance of considering



the  $f$ -dependence of the series elements of the test fixture, which allows to appropriately analyze the effect of the pads and other interconnects when either designing a prototype for probing or selecting the most appropriate de-embedding technique for a particular application.

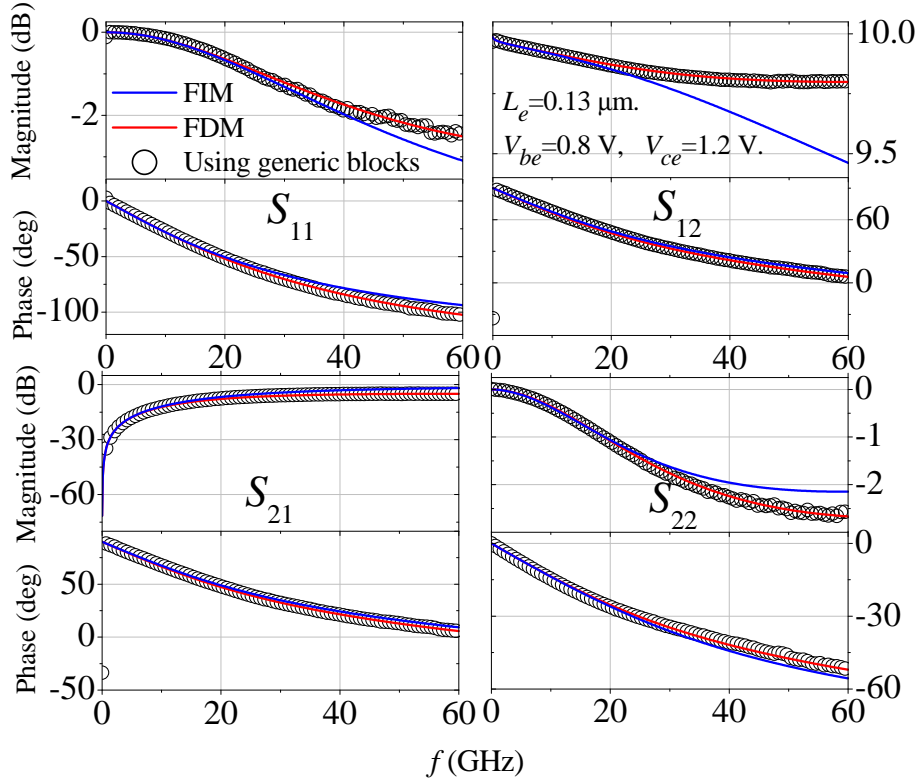


**Figure 2.10:**  $S$ -parameters for a de-embedded SiGe HBT under  $V_{be} = 0.8\text{ V}$  and  $V_{ce} = 2\text{ V}$  bias condition.

Thus, the presented procedures for modeling the test fixture and de-embedding its parasitic effects from raw measurements provides a solid starting point to analyze the non-linear effects present in the HBT, which will be treated in the subsequent sections.

## 2.5 Conclusions and Original Contributions

- A simple, accurate, and physically based methodology to obtain the model parameters for a ground-shielded test fixture was proposed, directly introducing for the first time the skin effect into a de-embedding procedure using frequency dependent parameters.
- The validity of this proposal was verified by correlating experimental and simulated data obtained from test fixtures with and without a DUT up to 60 GHz.
- It was demonstrated that using simple frequency independent representations for the test fixture introduces severe errors within the tens of gigahertz frequency range. Based on this fact, the proposed methodology represents a good alternative for modeling these structures at microwave frequencies while simultaneously maintaining accuracy, simplicity, and physical significance of the obtained parameters.

## Modeling the Distributed Physical Effects in Microwave SiGe HBTs

THE requirements of modern communication systems put stringent demands on semiconductor technologies for providing performance at a low cost [40]. BiCMOS technology based on SiGe HBTs provides an attractive solution to address these exigencies, due to its inherent properties, such as low noise, high linearity, and low power consumption. However, the first step to optimize the performance of these microwave ICs is the accurate determination of the device characteristics and its adequate incorporation in a practical simulation-model.

Most common bipolar models for circuit simulation use the Quasi-Static (QS) approximation, which assumes that the electrons and holes move with infinite velocity [41]. However, when the frequency rises and the transistor cannot follow external excitations instantaneously, the QS approximation misses the details of the response associated with the time required for minority carriers to propagate within a quasi-neutral region. Consequently, circuits designed using QS models might not be optimized for performance. Also, for small-signal applications, even the excess-phase extension of commonly used models [42, 43] fails to accurately describe the phase margin and stability of wide-band amplifiers. Thus, a Non-Quasi Static (NQS) interpretation is necessary to represent the HBT operating at high frequency [44].

In this regard, as it is illustrated in Fig. 3.1, it is possible to distinguish between: *i) vertical NQS effect*, which impacts the current crossing perpendicularly to the junctions and becomes noticeable when signal frequencies approach to the maximum common-emitter cut-off frequency,  $f_T$ ; and *ii) lateral NQS effects*, which are a consequence of the distributed RC nature in the lateral direction along the intrinsic junctions.

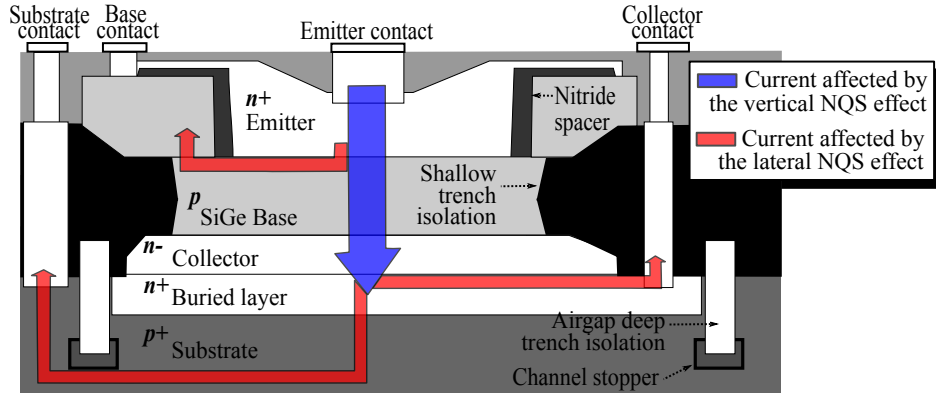


**Figure 3.1:** Sketch of an HBT cross section showing the currents influenced by the NQS effects.

NQS effects have been traditionally accounted for by modifying the existing compact models [45]. However, this leads to complicated models that are difficult to extract from measured data. Thus, a practical alternative to estimate the NQS effect influencing the electrical characteristics of the HBT, is using a distributed equivalent circuit. Fig. 3.2 shows a simplified sketch illustrating how the HBT structure can be represented using a distributed network, which considers the capacitances associated with the space charge layer at each side of the base region. These capacitances are referred to as base-emitter ( $C_{be}$ ), and base-collector ( $C_{bc}$ ) junction capacitances per unit length; the corresponding value depends on the doping profile and on the width of the associated depletion region.  $r_{bi}$  is the intrinsic base resistance, which is a function of the bias conditions since the width of the space charge layers determine the lateral resistance in the active base;  $g_{be}$  and  $g_{bc}$ , are the dynamic base-emitter and base-collector conductances, respectively; the depletion capacitance formed at the bottom of the sub-collector-substrate junction is represented by means of  $C_{sub}$ , whereas the influence of the in-

ner substrate resistance, and the additional resistances associated with the channel stopper and the substrate contacts are taken into account by  $r_{sub}$ .

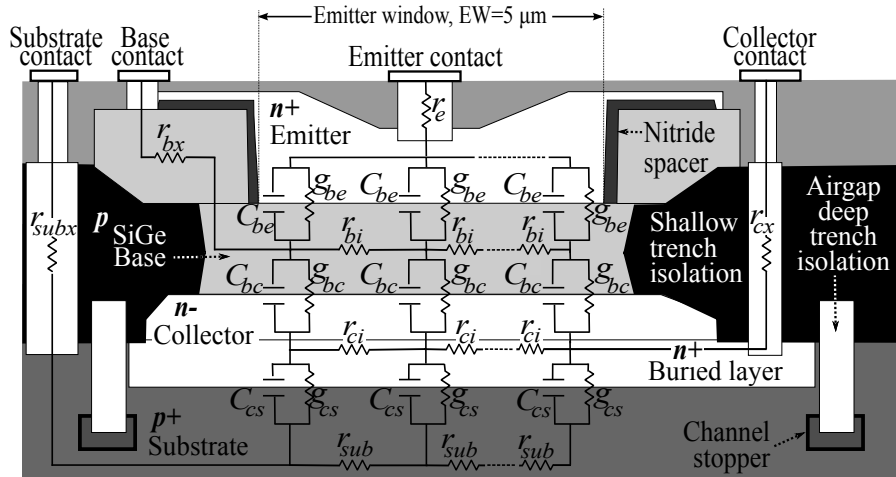


**Figure 3.2:** Cross section of an HBT showing the small-signal distributed equivalent circuit model.

As it will be shown further on, the correct representation of distributed effects plays a very important role in HBT modeling and characterization at HF; additionally, it is one of the most difficult challenges in device modeling since there is a compromise between accuracy and computing time when simulating RF-ICs. Therefore, a detailed analysis and determination methodology of these effects has to be performed to accurately predict HBT’s behavior when used for microwave applications.

### 3.1 Modeling the Electrical Characteristics of the HBT’s Output Port

As the frequency of operation increases for advanced high speed and RF circuits, the influence of substrate parasitic effects on HBT electrical performances cannot be neglected [46–48]. These parasitics strongly influence the HBT’s output characteristics. In this case, the output port is the collector terminal. Therefore, for advanced RF circuit design, the impact of the substrate effects must be correctly accounted for in the modeling of the HBT.

For an adequate modeling of the substrate effects, it is necessary to develop physically based models according to the device structure. In the simplest equivalent circuit, used in the current SGP model [49], only the depletion region around the buried layer is taken into account. As it is shown in Fig. 3.3, SGP models the substrate parasitics with a lumped junction capacitor  $Q_{scs}$ , whose value is approximated from the geometry of the buried layer.

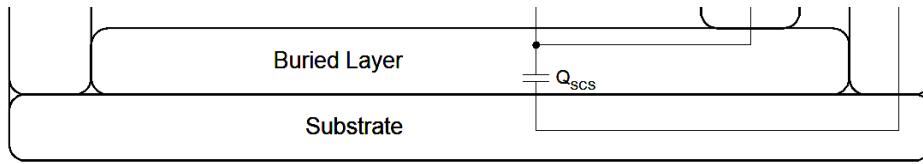


**Figure 3.3:** Sketch of an HBT cross section showing the SGP representation for the substrate parasitics.

However, the reliability of this approach is limited because it neglects the influence of the bulk substrate and the channel stopper resistances. To consider them, an additional resistor is usually connected in series to the sub-collector-substrate capacitance, as it is illustrated in Fig. 3.4, which considers  $C_{sub}$  connected in series to  $r_{sub}$ .

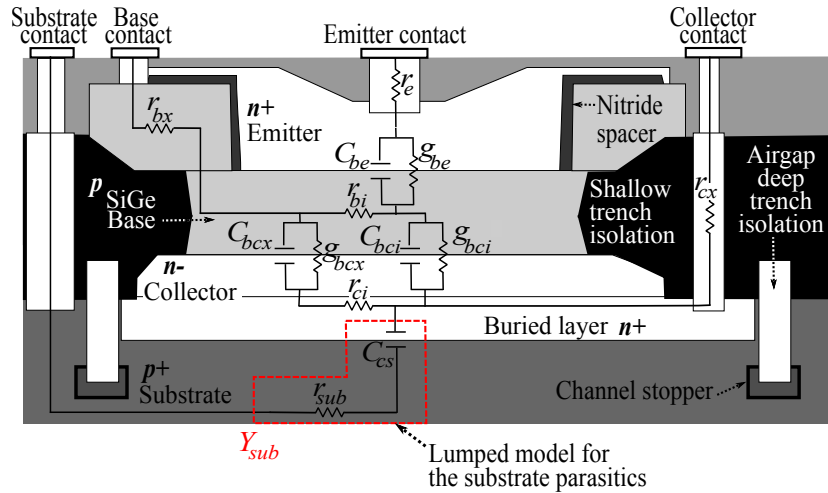


**Figure 3.4:** Sketch of an HBT cross section and its corresponding equivalent circuit model considering an RC-lumped model for the substrate network.

Also, the extrinsic resistances  $r_{bx}$ ,  $r_{cx}$ , and  $r_e$ ; the dynamic conductances  $g_{be}$ ,  $g_{bcx}$  and  $g_{bci}$ ; the intrinsic base resistance  $r_{bi}$ ; and the junction capacitances  $C_{be}$ ,  $C_{bcx}$ , and  $C_{bci}$ , are considered in this model. This approach is widely used in modern models such as MEXTRAM [50] or HICUM [11]; however, it is restricted for application at relatively low frequencies since when the frequency increases it is not accurate enough, yielding errors when representing the output impedance of the transistor and the actual gain [51].

Thus, in order to accurately model the electrical characteristics of the HBT's output, on-wafer two-port S-parameter measurements, using the procedure described in section 1.2, were performed on a common-emitter HBT fabricated on p-type Si substrate in a 0.13  $\mu\text{m}$  BiCMOS technology. As it is illustrated in Fig. 3.5, the DUT was biased at the cold condition, which is defined as the condition when the emitter-base junction and base-collector junction are zero biased (i.e.  $V_{be} = V_{ce} = 0$ ). Therefore, both junctions are depleted, resulting in a simplified equivalent circuit that allows a simple characterization of the substrate effects.

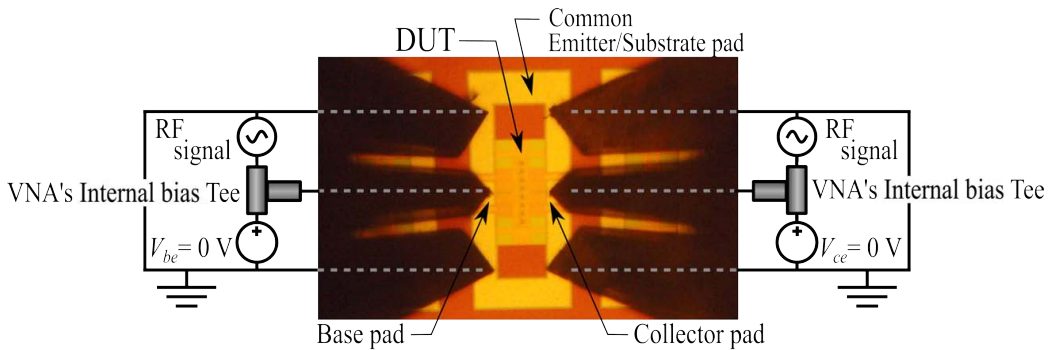


**Figure 3.5:** Micrograph showing the pad configuration of the HBT, illustrating the experimental array for RF characterization under the cold condition.

Once the S-parameters of the DUT have been obtained, they can be associated directly with the equivalent circuit model, and all the corresponding elements can be determined from these experimental data, as it is explained hereafter.

### 3.1.1 Proposed Model and Corresponding Extraction Methodology

When the HBT is biased in a cold condition, the following applies:

*i)* no potential drop is present at the contacts, *ii)* all the dynamic resistances present very large values, (i.e., no transfer current exists), and *iii)* there is no current gain. Therefore, in this case, the influence of the extrinsic and dynamic resistances can be neglected in the HBT equivalent circuit, resulting in the simplified model presented in Fig. 3.6.

Additionally, for an heterojunction bipolar transistor fabricated on a high-resistivity substrate, the value of the intrinsic base resistance is much lower than  $\text{Re}(Z_{sub})$ , where  $Z_{sub} = 1/Y_{sub}$ . Therefore, the influence of the intrinsic base resistance can be neglected in this case, simplifying the equivalent circuit to that illustrated in Fig. 3.7, where  $C_{bc}$  considers the combined effect of  $C_{bcx}$  and  $C_{bci}$ . Then, the constitutive parameters of the equivalent circuit illustrated in Fig. 3.7, can be extracted using the experimental Y-parameters, obtained from the corresponding transformation of the measured S-parameters.

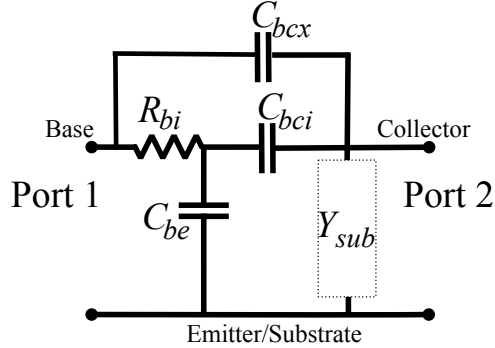


**Figure 3.6:** Small-signal equivalent circuit model for a SiGe HBT biased at  $V_{BE} = V_{BC} = 0$ .

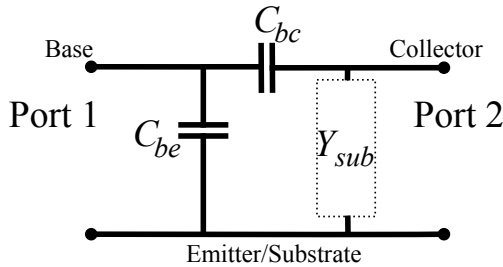


**Figure 3.7:** Simplified HBT model in common emitter configuration used to derive the proposed substrate model.

In this case, the following expressions can be written:

$$\text{Im}(Y_{11} + Y_{12}) = \omega C_{be} \quad (3.1)$$

$$-\text{Im}(Y_{12}) = \omega C_{bc} \quad (3.2)$$

Thus, plotting (3.1) and (3.2) versus  $\omega$ , the values of  $C_{be}$  and  $C_{bc}$



can be obtained from the respective slopes, as illustrated in Fig. 3.8.

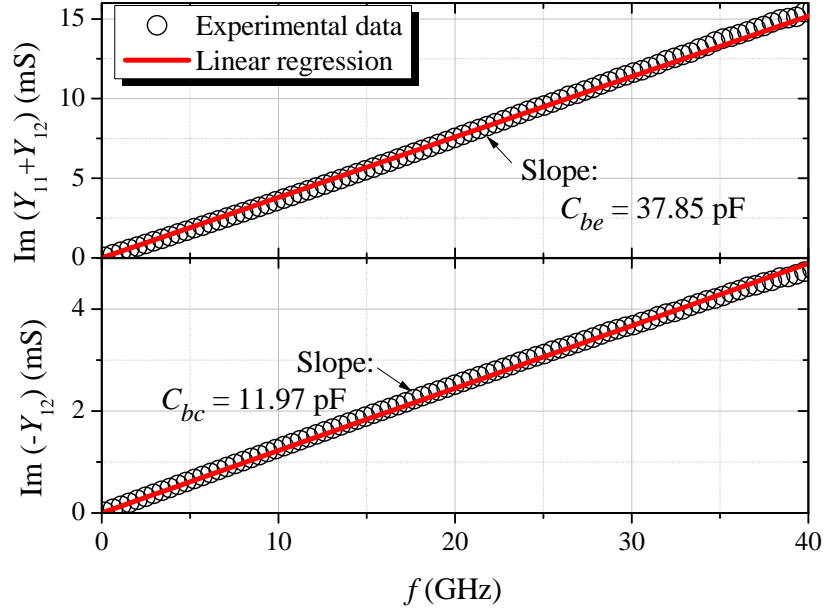


**Figure 3.8:** Linear regressions used to determine  $C_{be}$  and  $C_{bc}$ .

In accordance with the model shown in Fig. 3.7, the substrate admittance ( $Y_{sub}$ ) is related with the experimental data as:

$$Y_{sub} = Y_{12} + Y_{22} \quad (3.3)$$

To model the substrate admittance, it is important to carefully analyze the collector-substrate junction. In this regard, notice in Fig. 3.1 that the boundary conditions between the depletion region and the bulk substrate change as the channel stopper is closer. This implies that the peripheral capacitance differs from the bottom capacitance depending on the proximity of the channel stopper, and also on the variation of the potential along the depletion region, influencing also the local resistance of the bulk substrate. In consequence, in order to accurately model the substrate parasitics in an HBT, it is necessary to consider the corresponding effects using a distributed model, as illustrated in Fig. 3.9.

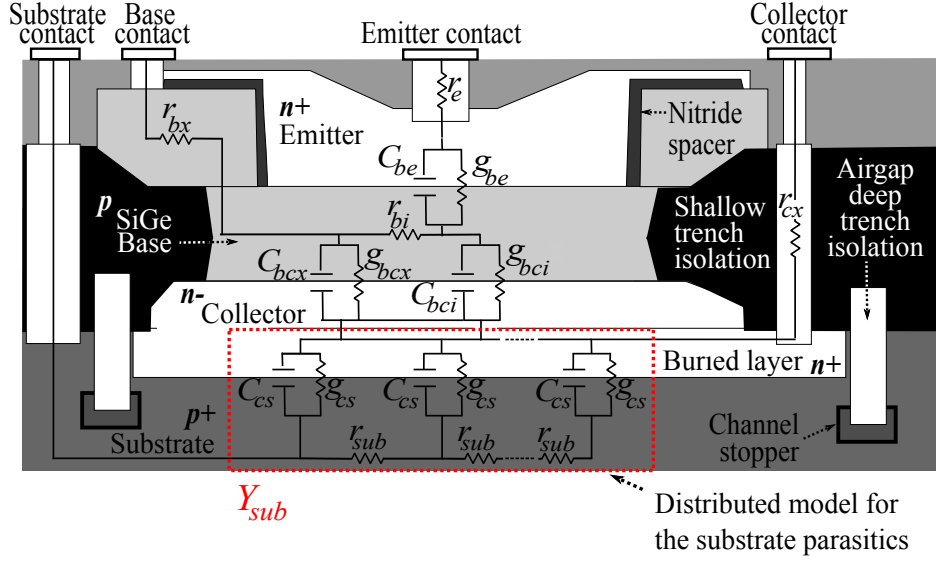


**Figure 3.9:** Sketch of an HBT cross section and its corresponding equivalent circuit considering a distributed model for the substrate network.

From [52, 53], it is possible to obtain an analytical expression for  $Y_{sub}$ , this is:

$$Y_{sub} = \sqrt{\frac{j\omega C_{cs}}{r_{sub}}} \tanh(\sqrt{j\omega r_{sub} C_{cs}}) \quad (3.4)$$

where the total distributed resistance and capacitance,  $r_{sub}$  and  $c_{sub}$  respectively, are given by:

$$\text{Re}(Y_{sub}) = \frac{\sqrt{2r_{sub}C_{cs}\omega}}{r_{sub}} \quad (3.5)$$

$$\text{Im}(Y_{sub})/\omega = C_{cs} \quad (3.6)$$

The resulting model, based on (3.5) and (3.6), is shown in Fig. 3.10, where it is possible to notice a good correlation with the experimental data.

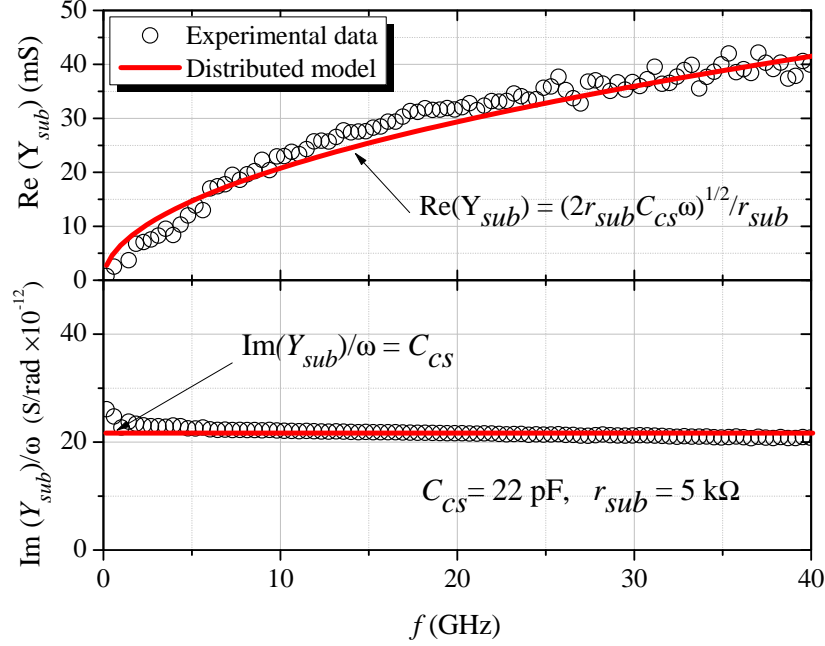


**Figure 3.10:** Frequency dependence of the substrate parasitics for a SiGe HBT under  $V_{BE} = V_{BC} = 0$  bias condition.

### 3.1.2 Model Verification

Taking into account that the  $S_{22}$  parameter is directly related with the output of the HBT and is strongly affected by the substrate parasitics. The usefulness of the proposed model and extraction method is verified by performing a simulation using the equivalent circuit shown in Fig. 3.7, and evaluating the accuracy of the lumped and distributed models for  $S_{22}$ . As shown in Fig. 3.11, a very good correlation between simulated and experimental data is achieved when the distributed model is used, reproducing both magnitude and phase and allowing to verify the accuracy and consistency of this proposal to represent the HBT-output characteristics.

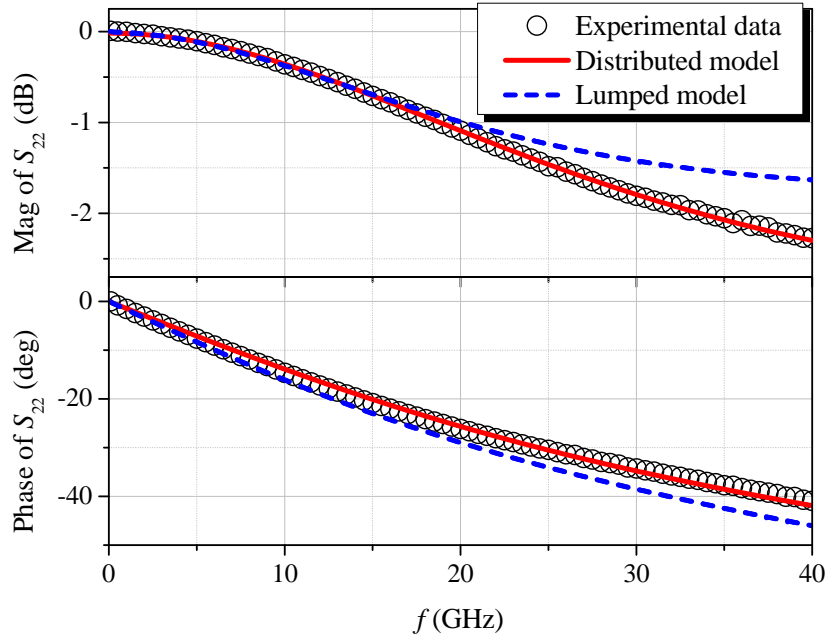


**Figure 3.11:** Comparison between experimental and simulated data for the  $S_{22}$ -parameter using a lumped and a distributed network to model the substrate parasitics in a SiGe HBT.

The construction of a microwave IC usually starts with a proper design of the transistor; then the matching networks of the input and output ports are determined for a particular stability and gain criteria. Thus, once that the output characteristics have been analyzed, the following section will deal with the analysis of the high frequency effects for the input impedance of the HBT.

### 3.2 Modeling the Electrical Characteristics in the HBT's Input

The input impedance of an HBT in the common-emitter configuration is usually difficult to predict either by compact or equivalent circuit models due to the NQS and distributed effects in the base region. These effects decrease the base admittance in magnitude when increasing the operation frequency as a result of a high-frequency internal biasing effect. However, applying

a rigorous transmission line analysis to the effects occurring in SiGe HBTs allows for a proper representation and physical model parameter extraction in a simple and straightforward way.

In this case, common-emitter SiGe HBTs were biased, as it is illustrated in Fig. 3.12, at  $V_E = V_C = 0$  V in order to analyze the parasitics associated with the base-to-emitter junction. This particular bias is selected since the effect of the collector current is negligible in the small-signal model when the device is operating under this condition.

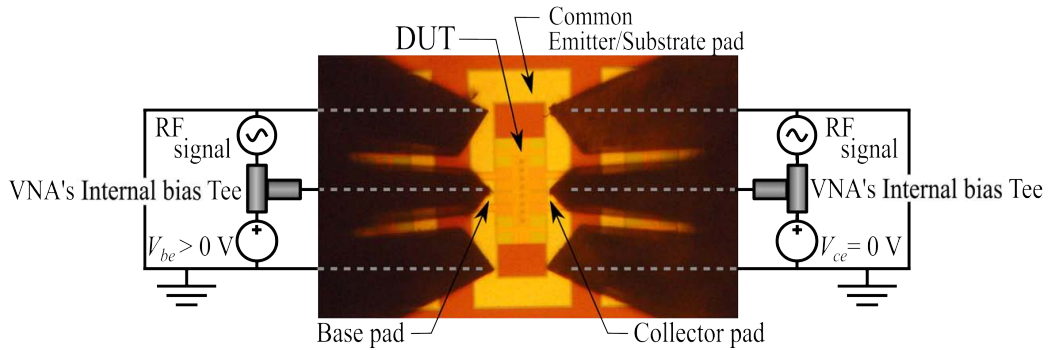


**Figure 3.12:** Micrograph showing the pad configuration of the HBT, illustrating the experimental array for RF characterization under  $V_{be} > 0$  V.

Again, S-parameter data used to develop the models proposed in the following section were performed using the experimental setup and procedure described in section 1.2.

### 3.2.1 Proposed Model and Corresponding Extraction Methodology

Once that the substrate effects have been removed from the experimental data, and assuming common emitter/bulk configuration, the HBT equivalent circuit in Fig. 3.2 at  $V_C = 0$  V, can be rearranged to the form shown in Fig. 3.13 (a). A further simplification of the circuit can be carried out when short-circuiting the collector and emitter terminals. In this case, the circuit in Fig. 3.13 (b) can be obtained.

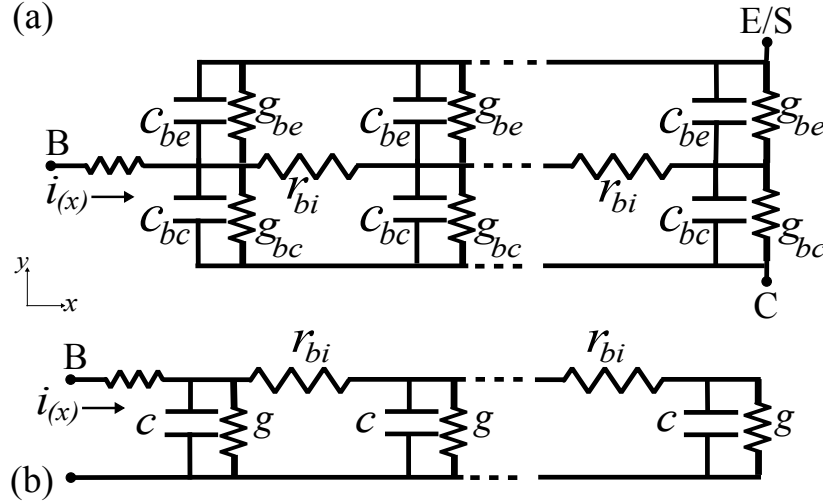


**Figure 3.13:** Simplified models: (a) assuming common emitter/substrate configuration at  $V_C = 0 V$ , and (b) assuming that the HBT is terminated in a short-circuit.

The model in Fig. 3.13 (b) represents the distributed nature of the base resistance and resembles an  $RCG$  transmission line. Hence, when the device is represented using this equivalent circuit, the distributed base resistance can be accurately analyzed at microwave frequencies using transmission line theory concepts.

Solving the telegraph equations associated with the circuit in Fig. 3.13 (b) for the voltage and current along the base of the HBT results in:

$$v(x) = \frac{V e^{j\omega t} \cosh(\gamma x)}{r_{bi} \cosh(\gamma x)} \quad (3.7)$$

$$i(x) = \frac{-\gamma V e^{j\omega t} \sinh(\gamma x)}{r_{bi} \sinh(\gamma x)} \quad (3.8)$$

where  $\gamma = \sqrt{r_{bi}(g + j\omega c)}$ . Thus, the input impedance for the device can be written using these equations; after a mathematical simplification it yields:

$$Z_{in} = \frac{v(x)}{i(x)} = \frac{\coth\left(x r_{bi} \sqrt{\frac{g + j\omega c}{r_{bi}}}\right)}{\sqrt{\frac{g + j\omega c}{r_{bi}}}} \quad (3.9)$$

which is a transmission line theory-based equation associated with the distributed base effects in an HBT.

To determine the  $RGC$  parameters involved in (3.9), this expression can be simplified by representing  $\coth(A + jB)$  by a Taylor series expansion:

$$\coth(A + jB) = \frac{\sum_{n=0}^{\infty} \frac{(A+jB)^{2n}}{(2n)!}}{\sum_{n=0}^{\infty} \frac{(A+jB)^{2n+1}}{(2n+1)!}} \quad (3.10)$$

and using two-terms in both the numerator and the denominator results in:

$$Z_{in} = \frac{xr_{bi}}{2} + \frac{1}{xg + j\omega xc} \quad (3.11)$$

This expression is equivalent to the equation for the short-circuit input impedance of the hybrid- $\pi$  circuit [21]. In fact, notice that this expression corresponds to a resistor ( $xr_{bi}$ ) in series with the parallel connection of a capacitor ( $xc$ ) and a conductor ( $xg$ ), which is the typical circuit representation used for the base of an HBT. Thus, it is clear that (3.11) is a second-order approximation of (3.9) which can be applied at relative low frequencies. For high frequencies, however, it might be necessary to include higher order terms to obtain accurate results. This will be discussed in the following section.

### 3.2.2 Results and Discussion

The input impedance associated with the circuit in Fig. 3.13 (b) corresponds to the HBT's  $Z_{11}$  parameter, which can be written in terms of  $r_{bi}$ ,  $c$ , and  $g$  at relatively low frequencies when assuming  $Z_{11} \approx Z_{in}$  (as defined in equation (3.12)). In this case,  $Z_{11}$  can be written as:

$$Z_{11} = \frac{2g + r_{bi}c^2\omega^2}{2\omega^2c^2} - j\frac{\omega c}{g^2 + c^2\omega^2} \quad (3.12)$$

From the real and imaginary parts of  $Z_{11}$ , the following expressions can be obtained:

$$\frac{-\omega}{\text{Im}(Z_{11})} = \frac{g^2}{c} + c\omega^2 \quad (3.13)$$

$$2(\text{Re}(Z_{11})\omega^2 - \frac{g}{c^2}) = r_{bi}\omega^2 \quad (3.14)$$

Then, after transforming the measured S-parameters of an HBT to Z-parameters, a linear regression of the experimental  $-\omega/\text{Im}(Z_{11})$  versus  $\omega^2$  data can be performed. Using this regression,  $c$  and  $g$  can be respectively obtained from the corresponding slope and intercept with the abscises as shown in Fig. 3.14.

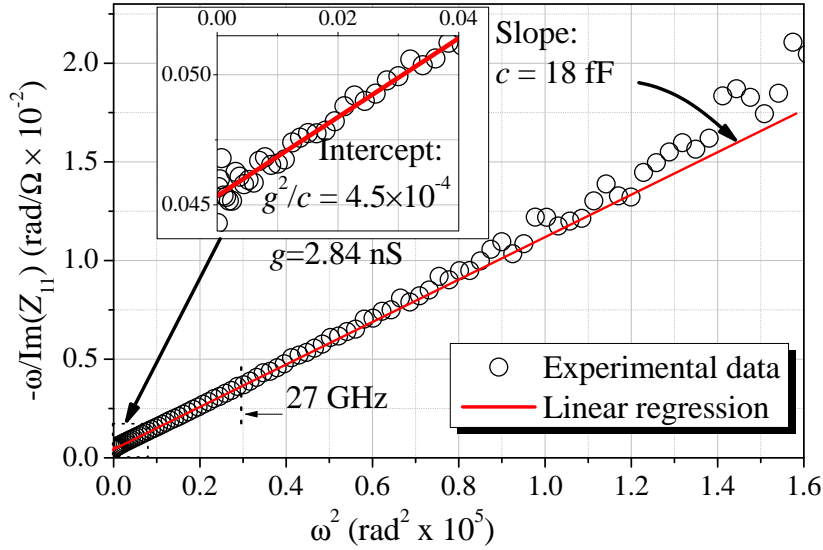


Figure 3.14: Linear regression used to determine  $g$  and  $c$ .

Once that the  $c$  and  $g$  parameters are known, the linear regression of the experimental  $2(\text{Re}(Z_{11})\omega^2 - g/c^2)$  versus  $\omega^2$  can be used to determine  $r_{bi}$ , as illustrated in Fig. 3.15.



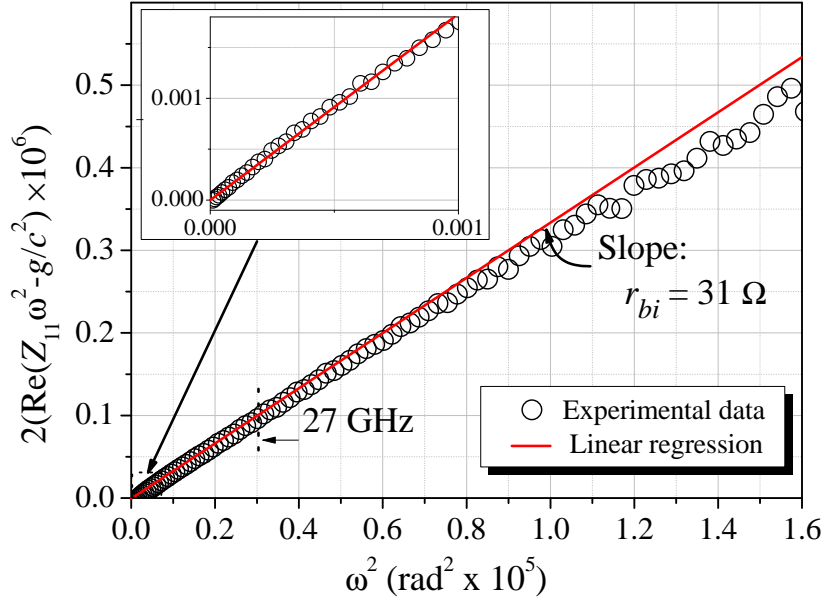


Figure 3.15: Linear regression used to determine  $r_{bi}$ .

Notice the excellent linearity of the experimental data at relatively low frequencies (up to about 27 GHz) for both regressions. However, as the frequency rises, the two-term approximation loses validity and deviates from the experimental data, which means that more terms in the expansion expressed by 3.10 should be considered. Nonetheless, additional terms involve the very same parameters extracted at low frequencies, allowing to easily implement a more accurate model by including addends to the expansion given in 3.10. Alternatively, equation 3.9 can be directly used in the simulation to obtain the most accurate results that this model may yield.

Figs. 3.16 and 3.17 show that when using eq. (3.9) excellent model-experiment correlation is achieved when representing the complex  $Z_{11}$  up to 60 GHz. In contrast, when using the simple and widely known  $\pi$ -model, the experimental  $Z_{11}$  parameter data is appropriately reproduced only up to around 27 GHz.

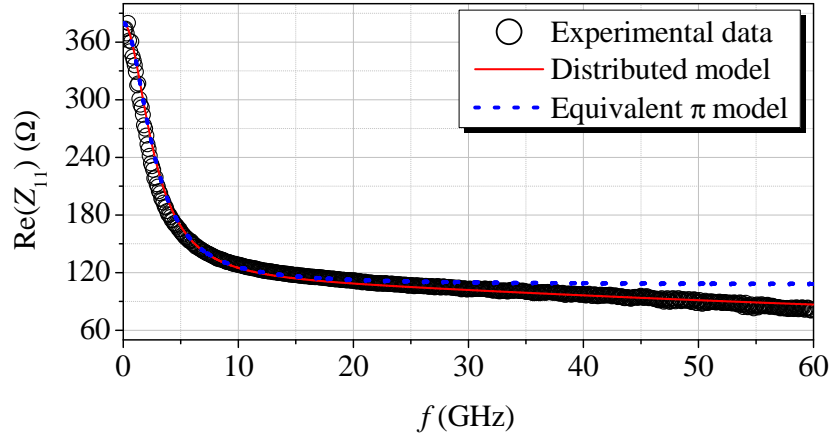


Figure 3.16: Simulation-experiment correlation for the real part of  $Z_{11}$ .

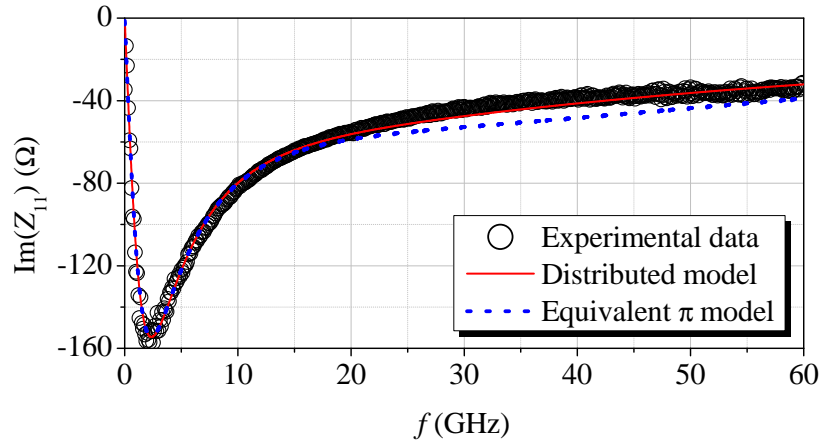


Figure 3.17: Simulation-experiment correlation for the imaginary part of  $Z_{11}$ .

### 3.3 Conclusions and Original Contributions

Commonly, the active base region effects and the substrate parasitic effects in a SiGe HBT are modeled for small-signal operation using a traditional lumped  $\pi$ -circuit model. However, the limitations of this model for high frequency representation of the base and substrate effects in an HBT were evidenced in this study. This is essentially because the distributed nature

effects are not considered.

Thus, through a novel analytical extraction method, proposed to determine the constitutive parameters of a transmission line model from S-parameter measurements, the frequency range where the simple  $\pi$  model is valid has been determined for a SiGe HBT, obtaining that for frequencies beyond 20 GHz for the output and 27 GHz for the input, a more complete model is required for an accurate circuit behavior prediction. In this case, a very good simulation-experiment correlation for the input electrical characteristics of the HBT up to 60 GHz has been obtained using a complete distributed model.

Therefore, the proposed models for the HBT's characteristics, represent an important contribution in the field of physics-based equivalent circuit modeling since it helps to understand the substrate effects. The proposal can be used for improving integrated circuit design, evaluating the process technology and for optimizing the device structure.

## Improving the Modeling for Power Amplification in CE and CB SiGe HBTs

SiGe HBTs are currently used in wireless technologies due to their remarkable characteristics for power amplification at microwave frequencies [54]. One of the most important parameters in these applications is the HBT's maximum available power gain (MAG) [17]. For this reason, common-emitter (CE) and common-base (CB) configurations have been widely analyzed [55–57], showing that an HBT in CB configuration may provide higher power gain at high frequencies than in the CE configuration. This has been studied in detail through 2-D simulations for different base doping profiles [58], which allows determining the more suitable configuration for particular applications to reduce the amplification stages and improve the efficiency of power amplifiers. In consequence, since HBTs operating in different configurations might be present in the same circuit, IC designers require a reliable model that consistently represents the device in both cases.

Thus, motivated by the need of representations that can be indistinguishably used in CB and CE configurations, an analytical modeling and parameter extraction methodology for HBTs operating in these configurations is proposed in this chapter. Using the proposed models, the MAG for each one is accurately calculated, obtaining an excellent experiment-model correlation. Moreover, the frequency range for better power amplification for each configuration as a function of design parameters is determined, which

can be very helpful as a guide for HBT-IC design in the microwave range.

In this regard, in order to analyze the physical characteristics for power amplification, both CE as CB configured HBTs, on-wafer two-port S-parameter measurements were performed to a set of *npn* SiGe HBTs with emitter width,  $W_e=0.13 \mu\text{m}$ , and emitter lengths  $L_e=0.25 \mu\text{m}$ ,  $0.3 \mu\text{m}$ ,  $0.35 \mu\text{m}$ ,  $0.75 \mu\text{m}$ , and  $1 \mu\text{m}$ , were fabricated in an advanced  $0.13 \mu\text{m}$  BiCMOS technology. Furthermore, devices presenting these dimensions were configured in both CE and CB to analyze the corresponding response. In order to do so, on-wafer two-port S-parameter measurements were performed up to 60 GHz using the experimental setup and procedure described in section 1.2, In addition, the pad parasitics were also de-embedded using a two-step procedure and the corresponding dummy structures. The measurements were performed at different bias conditions, according to the requirements of the methods described in subsequent sections.

### 4.1 Determination of the HBT's Substrate Parasitics

The substrate parasitics considerably affect the performance of HBTs at high-frequency. Therefore, the associated equivalent circuit has to be determined to implement the HBT model, which is usually achieved by biasing the device under the cold condition ( $V_{be} = 0 \text{ V}$ , and  $V_{ce} = 0 \text{ V}$ ), and considering that the corresponding elements are bias independent [59, 60].

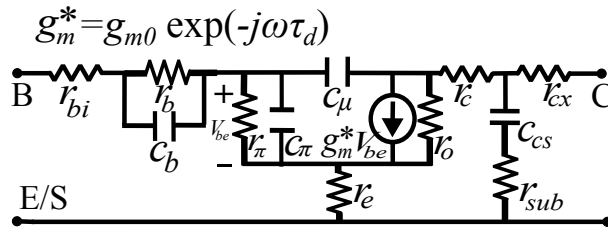


Figure 4.1: Small-signal equivalent circuit model for a CE SiGe HBT.

However, although the elements in the substrate network are roughly independent of  $V_{be}$ , they exhibit a strong dependence on  $V_{ce}$  as shown hereafter, which requires a careful model implementation at different bias conditions.

The substrate effects can be modeled by the collector-substrate depletion capacitance ( $C_{CS}$ ) and the substrate resistance ( $r_{sub}$ ), as shown in Fig. 4.1. In this case, after transforming the experimental S-parameters to Y-parameters,  $C_{CS} = -1/\omega \text{Im}(1/Y_{sub})$  and  $r_{sub} = \text{Re}(1/Y_{sub})$  can be obtained at different  $V_{ce}$  voltages when defining the substrate admittance as:

$$Y_{sub} = Y_{22} - Y_{11} \quad (4.1)$$

Notice in Fig.4.1 that determining the substrate elements in this fashion is valid provided that  $r_{cx} \ll |1/Y_{sub}|$ , which is a reasonable assumption in typical HBTs [61–63]. Thus, defining  $Z_{sub} = 1/Y_{sub}$ , and plotting  $\text{Re}(Z_{sub})$  and  $-1/\text{Im}(Z_{sub})$  versus  $\omega$ , the values of  $r_{sub}$  and  $C_{CS}$  can be obtained as is illustrated in Fig. 4.2.

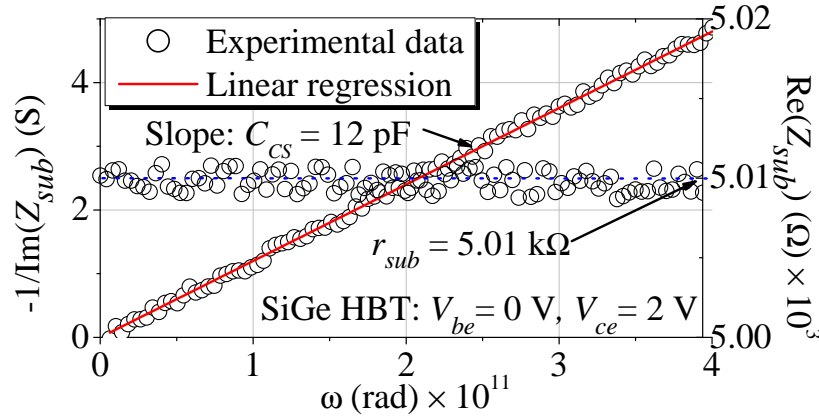
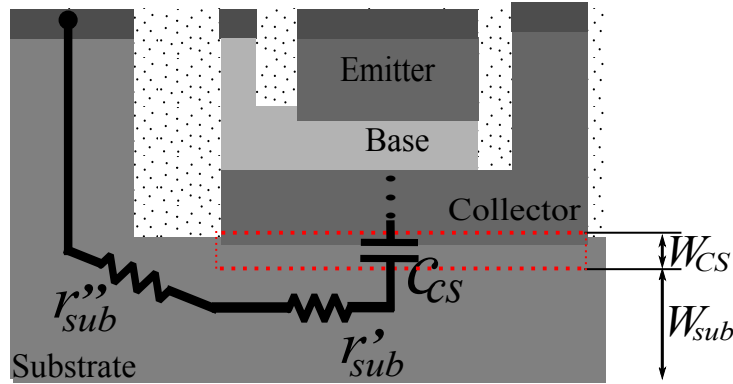


Figure 4.2: Linear regression used to determine  $C_{CS}$  and  $r_{sub}$ .

Even though strictly speaking  $r_{sub}$  is bias dependent, this is a partial dependence due to only part of the substrate resistance is influenced for the  $V_{ce}$  voltage. To illustrate the bias dependence of the collector-substrate capacitance and the substrate resistance ( $r_{sub} = r'_{sub} + r''_{sub}$ ), it is necessary to analyze the effect when the reverse bias voltage across the collector-substrate junction is increased. In this case, the depletion width  $W_{CS}$  increases, reducing the neutral region  $W_{sub}$ , leading in turn to the reduction of  $C_{CS}$ . Thus, a reduction of  $r'_{sub}$ , that is the portion of the  $r_{sub}$  influenced by the applied voltage, is also expected.



**Figure 4.3:** Cross-sectional view an HBT illustrating the substrate resistance components.

However, this variation is not significant in the total substrate resistance, being a very small portion of the total substrate resistance in this case, as is shown in Fig. 4.4. Therefore, it is possible to use an effective value for  $r_{sub}$  without compromising the accuracy in the results.

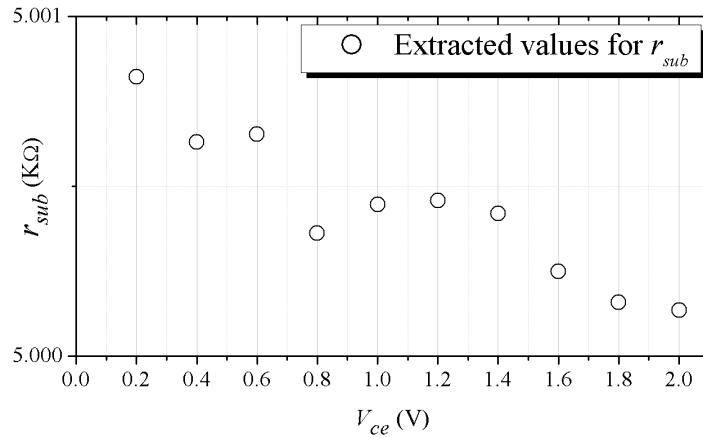


**Figure 4.4:** Bias dependence of  $r_{sub}$ .

Fig. 4.5 shows that the  $C_{CS}$  versus  $V_{ce}$  data obtained for a CE-configured HBT is correlated well by:

$$C_{CS} = C_{CS0} \left( 1 - \frac{V_{cs}}{V_{jcs}} \right)^{-m} \quad (4.2)$$

where  $C_{CS0}$  is the junction capacitance at zero bias,  $V_{jcs}$  is the built-in voltage,  $m$  is a grading exponent, and  $V_{cs}$  is the applied voltage.

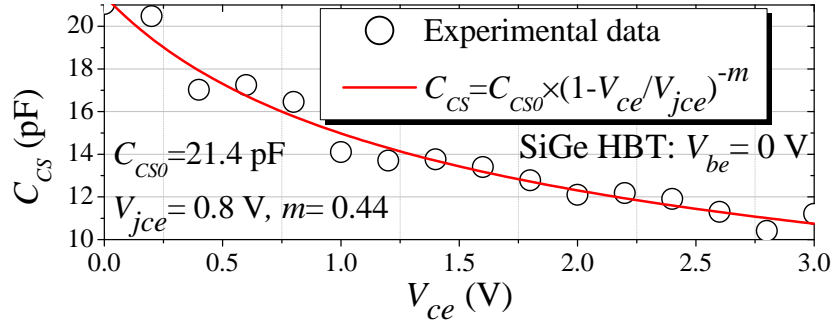


Figure 4.5: Extracted  $C_{CS}$  as a function of the applied collector voltage.

In accordance to Fig. 4.5, the collector-substrate depletion width increases due to an increasing reverse bias across the junction. Therefore, the width of the neutral region reduces, leading to the increase of  $C_{CS}$ , and showing a considerable difference between  $C_{CS}$  obtained at  $V_{ce}=0$  V (i.e., the cold condition) and obtained at voltages required for normal operation (e.g.,  $V_{ce}=2$  V). This points out that  $C_{CS}$  has to be considered as bias dependent to implement accurate and physically meaningful models.

## 4.2 Modeling the HBT in the Active Region

Once the substrate effects have been determined, they can be de-embedded from the experimental data. Fig. 4.6 shows the small-signal equivalent circuit for an HBT operating in the active region after removing the substrate effects.

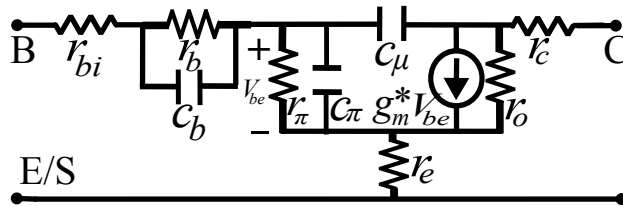


Figure 4.6: Small-signal equivalent circuit model for a CE SiGe HBT biased at  $V_{BE} > 0$  and  $V_{CE} = 2$  V.



In accordance with this circuit, its corresponding Z-parameters can be written as:

$$Z_{11} = r_{bi} + Z_b + \frac{Z_\pi}{1 + g_m^* Z_\pi} + r_e \quad (4.3)$$

$$Z_{12} = r_e + \frac{Z_\pi}{1 + g_m^* Z_\pi} \quad (4.4)$$

$$Z_{21} = r_e + \frac{Z_\pi}{1 + g_m^* Z_\pi} (1 - g_m^* Z_\mu) \quad (4.5)$$

$$Z_{22} = r_c + r_e + Z_\mu + \frac{Z_\pi}{1 + g_m^* Z_\pi} (1 - g_m^* Z_\mu) \quad (4.6)$$

where  $Z_b = r_b/(1 + j\omega C_b r_b)$ ;  $Z_\pi = r_\pi/(1 + j\omega C_\pi r_\pi)$ ;  $Z_\mu = 1/(j\omega C_\mu)$ ;  $\omega$  is the angular frequency, and  $j^2 = -1$ . Thus, using (4.3) through (4.6) the constitutive elements of the model can be obtained as follows.

Equations 4.5 and 4.6 can be rearranged such that:

$$\text{Re}(Z_{22} - Z_{21}) - \frac{1}{\text{Im}(Z_{22} - Z_{21})} = r_c + \omega C_\mu \quad (4.7)$$

As is illustrated in Fig. 4.7, after performing a linear regression of  $\text{Re}(Z_{22} - Z_{21}) - 1/(\text{Im}(Z_{22} - Z_{21}))$  versus  $\omega$ , the values of  $r_c$  and  $C_\mu$  can be extracted from the corresponding intercept and slope, respectively.

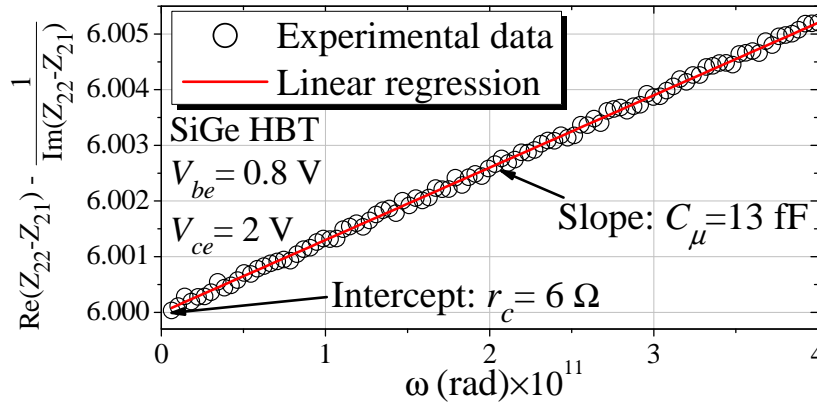


Figure 4.7: Linear regression used to determine  $r_c$  and  $C_\mu$ .

Similarly, using 4.3 and 4.4 allows to define:

$$-\frac{\omega}{\text{Im}(Z_{11} - Z_{12})} = \frac{1}{C_b r_b^2} + C_b \omega^2 \quad (4.8)$$

In this case, when performing a linear regression of  $-\omega/\text{Im}(Z_{11} - Z_{12})$  versus  $\omega^2$ ,  $C_b$  can be obtained directly from the respective slope, and  $r_b$  can be calculated as:  $r_b = 1/\sqrt{b \times m}$ , as shown in Fig. 4.8.

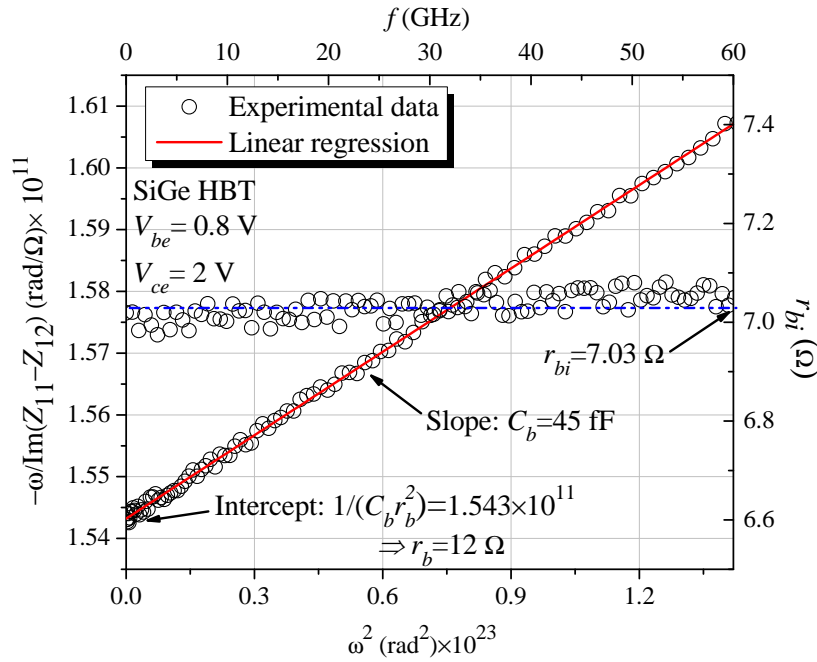


Figure 4.8: Linear regression used to determine  $r_b, C_b$  and  $r_{bi}$ .

Once that  $C_b$  and  $r_b$  have been obtained, the value of  $r_{bi}$  can be obtained using equation (4.9), as is illustrated in Fig. 4.8.

$$r_{bi} = \text{Re}(Z_{11} - Z_{12}) - \frac{r_b}{1 + C_b^2 r_b^2 \omega^2} \quad (4.9)$$

Finally, defining:

$$-\frac{\omega}{\text{Im}(Z_{12})} = \frac{(1 + g_{m0}r_{\pi})^2}{r_{\pi}^2(C_{\pi} - \tau_d)} + (C_{\pi} - \tau_d)\omega^2 \quad (4.10)$$

$$-\frac{\omega \text{Re}(Z_{12})}{\text{Im}(Z_{12})} = \frac{(1 + g_{m0}r_{\pi})(r_e + r_{\pi} + g_{m0}r_{\pi}r_e)}{(C_{\pi} - \tau_d)r_{\pi}^2} + (C_{\pi} - \tau_d)r_e\omega^2 \quad (4.11)$$

and performing linear regressions of  $-\omega/\text{Im}(Z_{12})$  and  $-\omega \text{Re}(Z_{12})/\text{Im}(Z_{12})$  as a function of  $\omega^2$ , the slopes  $m_1$  and  $m_2$ , and the intercepts  $b_1$  and  $b_2$  are determined respectively, as is shown in Figs. 4.9 and 4.10.

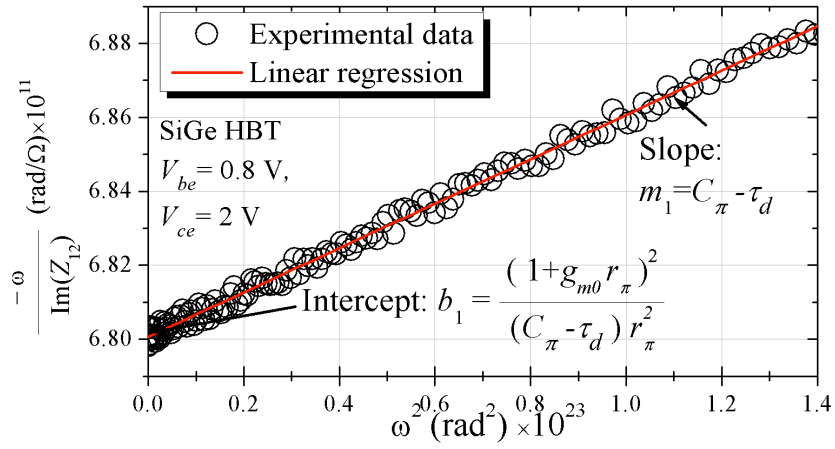


Figure 4.9: Linear regression, based on equation 4.10.

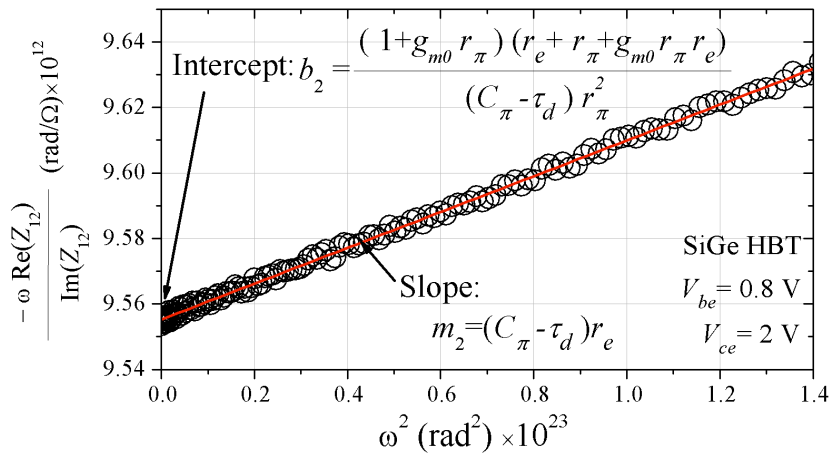


Figure 4.10: Linear regression, based on equation 4.11.

Thus,  $r_e$  is obtained from any of the associated slopes, whereas  $C_\pi$  and  $r_\pi$  are found by solving a system of equations involving the intercepts with the ordinates, whereas  $\tau_d$  and  $g_{m0}$  are given by:

$$g_{m0} = \omega C_\mu \operatorname{Im} \left( \frac{Z_{21} - r_e}{Z_{12} - r_e} \right) \quad (4.12)$$

$$\tau_d = C_\mu \left( \operatorname{Re} \left( \frac{Z_{21} - r_e}{Z_{12} - r_e} \right) - 1 \right) \quad (4.13)$$

From the data measured on the HBT in the CE configuration and biased at  $V_{be} = 0.8 \text{ V}$  and  $V_{ce} = 2 \text{ V}$ , the values shown in Table 4.1 were obtained when applying the proposed methodology.

$r_c = 6 \Omega$	$r_{bi} = 7.03 \Omega$	$r_b = 12 \Omega$	$C_\mu = 13 \text{ fF}$
$r_e = 9.1 \Omega$	$r_\pi = 814 \Omega$	$g_{m0} = 80 \text{ mS}$	$C_\pi = 60 \text{ fF}$

**Table 4.1:** Extracted parameters for a SiGe HBT biased at  $V_{BE} = 0.8$  and  $V_{CE} = 2 \text{ V}$ .

### 4.3 Dependence of Power Gain on Base Impedance

One of the advantages of the extraction method described in the previous section relies on the fact that the hybrid- $\pi$  model shown in Fig. 4.1 provides a representation of the small-signal behavior of the transistor, which is achieved independently of the circuit configuration; therefore, it is possible to use the same values for the parameters in both the CE and CB configurations. However, for the common-base configuration, the hybrid- $\pi$  model is somewhat cumbersome since the voltage-dependent current source is connected between the input and output terminals. Thus, the analysis corresponding to the common-base configuration can be simplified if the model in Fig. 4.1 is slightly modified.

First, notice in Fig. 4.1 that the voltage-dependent current source is connected from the intrinsic collector to the intrinsic emitter terminal. Nevertheless, the circuit behavior is unchanged if this single current source is replaced

by two current sources presenting the same value, one going from the intrinsic collector to the intrinsic base and another going from the intrinsic base to the intrinsic emitter. This is shown in Fig. 4.11.

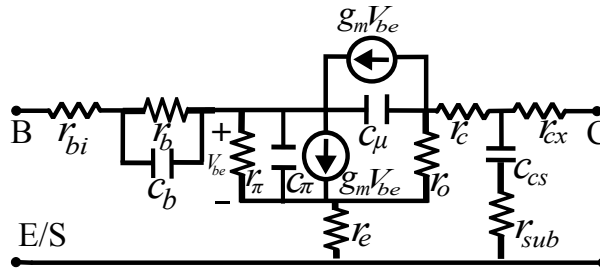


Figure 4.11: Modified Hybrid- $\pi$  model for CE SiGe HBT.

When applying Kirchoff's current law at the intrinsic base and at the intrinsic collector, it is possible to verify that the equations that describe the operation of these circuits are identical. Moreover, notice that the controlled current source connecting the intrinsic base and the intrinsic emitter is controlled by the voltage at its terminals (i.e., it is no longer a transconductance but a conductance). Therefore, this current source can be replaced by a resistor of value  $1/g_m$ . This resistance appears in parallel with  $r_\pi$ , and the parallel combination of the two is called  $r_{\pi e} = r_\pi || 1/g_m$ . This new equivalent circuit is shown in Fig. 4.12a, which can be redrawn as shown in Fig. 4.12b, obtaining a simplified circuit which allows carrying out the analysis presented afterwards.

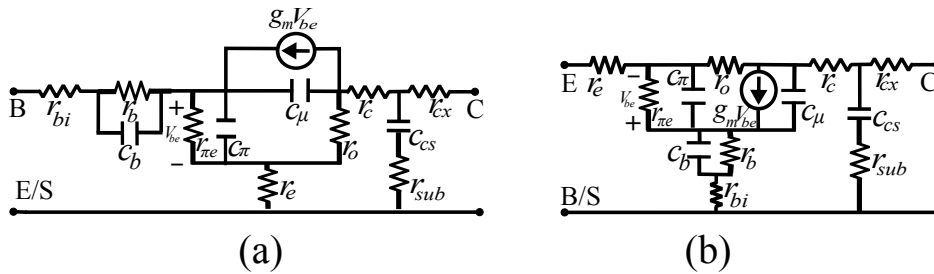
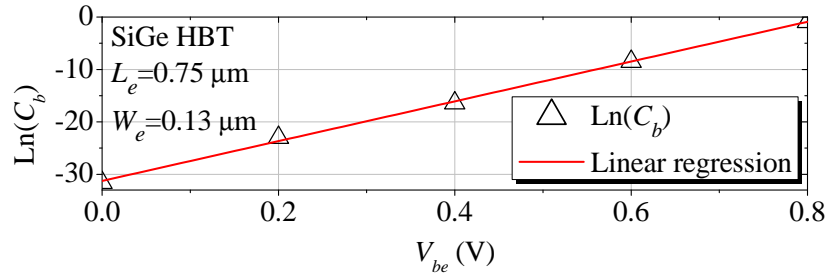


Figure 4.12: Equivalent model for (a) CE (b) CB.

In [58], the superior power gain of CB-configured HBTs at relatively high frequencies is attributed to a reduction of  $r_b$  to values that are comparable to  $r_e$ . In this case, the effective base impedance is assumed to be purely real

(i.e.,  $Z_b \approx r_b$ ). However, in practice  $Z_b$  presents a complex value influenced by the diffusion capacitance  $C_b$  associated with the base region. Thus, in accordance to Fig.4.1 and Fig. 4.12b,  $Z_b = r_{bi} + r_b || 1/j\omega C_b$  must be considered to model MAG for microwave HBTs. In fact,  $C_b$  extracted from experimental data using the proposed method exhibits the exponential trend expected for a diffusion capacitance, as shown in Fig 4.13. Therefore, the frequency and bias dependence of  $Z_b$  has to be taken into account when defining the operation conditions at which the CB configuration is more suitable for power amplification than the CE configuration. This is achieved by implementing the models in Figs. 4.1 and Fig. 4.12b using the proposed extraction methodology.



**Figure 4.13:** Extracted  $C_b$  as a function of the applied voltage.

In order to define the frequency ranges of applicability of the CB and CE configurations, MAG has to be determined using either experimental or simulated S-parameters. In this case, the following equation has to be applied:

$$\text{MAG} = \text{MSG}(K - \sqrt{K^2 - 1}) \quad (4.14)$$

where MSG is the maximum stable gain, expressed as:  $\text{MSG} = |S_{12}|/|S_{21}|$ ; and  $K$  is Rollet's stability factor [64], given as:

$$K = \frac{1 - |S_{11}|^2 - |S_{22}|^2 + |S_{11}S_{22} - S_{12}S_{21}|^2}{2|S_{12}S_{21}|} \quad (4.15)$$

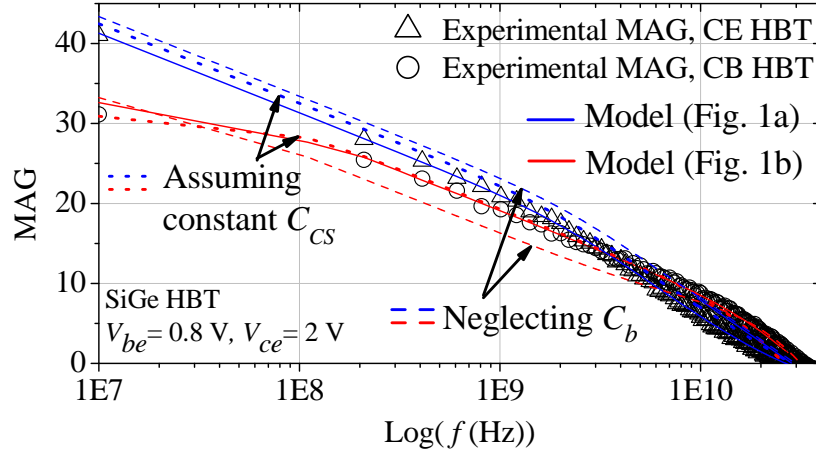


**Figure 4.14:** Experimental and simulated MAG for CE and CB-configured SiGe HBTs showing the effect of neglecting  $C_b$  and the bias dependence of  $C_{CS}$ .

Thus, using the model in Fig. 4.1, MAG for the CB and CE configurations can be obtained from (4.15). As shown in Fig. 4.14, excellent simulation-experiment correlation is obtained for both configurations using the same values for the model parameters, validating the proposed methodology. Notice also in Fig. 4.14 that neglecting either the complex value of  $Z_b$  by ignoring  $C_b$  or neglecting the bias dependence of  $C_{CS}$  introduces an error in the model for both configurations.

Fig. 4.15 shows the crossover frequency ( $f_A$ ) above which MAG for the CB configuration is higher than MAG for the CE configuration. Observe in this figure that  $f_A$  is smaller than the maximum frequency of oscillation ( $f_{max}$ ). This indicates that operating the device in the CB configuration rather than in the CE configuration is preferable within a considerable frequency range beyond  $f_A$ , at which power amplification occurs. Moreover, this frequency range is accurately predicted using the model implementation proposed here.

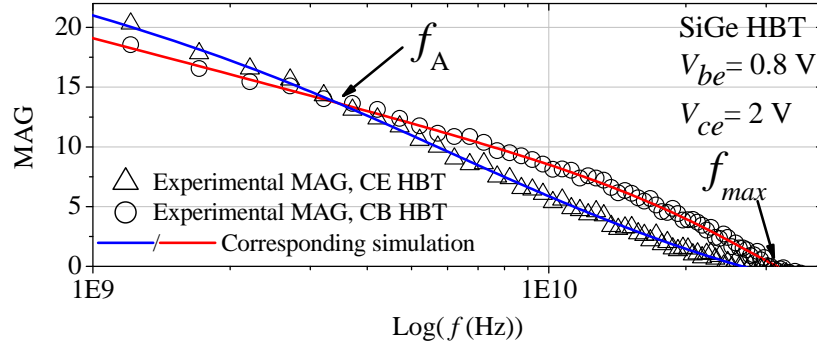


**Figure 4.15:** Experimental and simulated power gain curves showing  $f_A \approx 2.5$  GHz and  $f_{max} \approx 24$  GHz.

Going further into the analysis, an expression to determine  $f_A$  was proposed in [58]. However, this expression involves the cutoff frequency ( $f_T$ ) of the CE configuration. Unfortunately,  $f_T$  is a figure of merit related to the intrinsic part of the device and provides no information about the terminal impedances seen by the flowing charge. In this regard, an expression that includes the delay effects associated with the complex  $Z_b$  is required.

In order to find  $f_A$ , it is necessary to obtain an analytical expression for  $MAG_{CE}$  and  $MAG_{CB}$ . For this purpose, the forward and reverse hybrid parameters (h-parameters), for CE and CB models are used. Thus, using the model shown in Fig. 4.1 the following expressions are obtained:

$$h_{21CE} = \frac{\frac{g_m Z_1}{j\omega C_\mu} - Z_1 - r_e(1 + g_m Z_1)}{\frac{1}{j\omega C_\mu} + Z_1 + (r_e + r_c)(1 + g_m Z_1)} \quad (4.16)$$

$$h_{12CE} = \frac{r_e(1 + g_m Z_1) + Z_1}{\frac{1}{j\omega C_\mu} + Z_1 + (r_e + r_c)(1 + g_m Z_1)} \quad (4.17)$$

where  $Z_1$  is given by  $Z_1 = r_\pi / (1 + j\omega r_\pi C_\pi)$ . In a similar way, using the model shown in Fig. 4.12b:

$$h_{21CB} = -\frac{g_m Z_2 + j\omega Z_b C_\mu}{1 + j\omega C_\mu (Z_b + r_c)} \quad (4.18)$$

$$h_{12CB} = \frac{j\omega C_\mu Z_b}{Z_b(1 + g_m) + j\omega C_\mu (Z_b + r_c)} \quad (4.19)$$



where  $Z_2$  is given by  $Z_2 = r_{\pi e}/(1 + j\omega r_{\pi e} C_{\pi})$  and  $r_{\pi e} = 1/(g_m + 1/r_{\pi})$ .

From (4.15)  $K \approx 1$ , therefore, equations (4.16) to (4.19) can be used to calculate  $MAG_{CE}$  and  $MAG_{CB}$  from:

$$MAG_{CB} \approx \frac{|h_{21CE}|}{|h_{12CE}|} \approx \left| \frac{jg_m Z_1}{C_{\mu}(r_e + Z_1 + g_m r_e Z_1)\omega} \right| \quad (4.20)$$

$$MAG_{CE} \approx \frac{|h_{21CB}|}{|h_{12CB}|} \approx \left| \frac{(g_m Z_2 + jC_{\mu} Z_b \omega)((1 + g_m)Z_b + jC_{\mu}(r_c + Z_b)\omega)}{C_{\mu} Z_b \omega(-j + C_{\mu}(r_c + Z_b)\omega)} \right| \quad (4.21)$$

Thus, equating the  $MAG_{CE}$  and  $MAG_{CB}$  and solving for  $f_A$ , the following expression can be obtained after some simplifications:

$$f_A = \left( C_b r_b - 2\pi \sqrt{C_b C_{\mu} r_b (r_c - r_e/2)} + C_{\mu} (3r_b + r_c) \right)^{-1} \quad (4.22)$$

As shown in Fig. 4.16, equation (4.22) accurately represents the experimentally obtained  $f_A$  for devices with different geometry (i.e., varying the area of the emitter) and at different  $V_{be}$ .

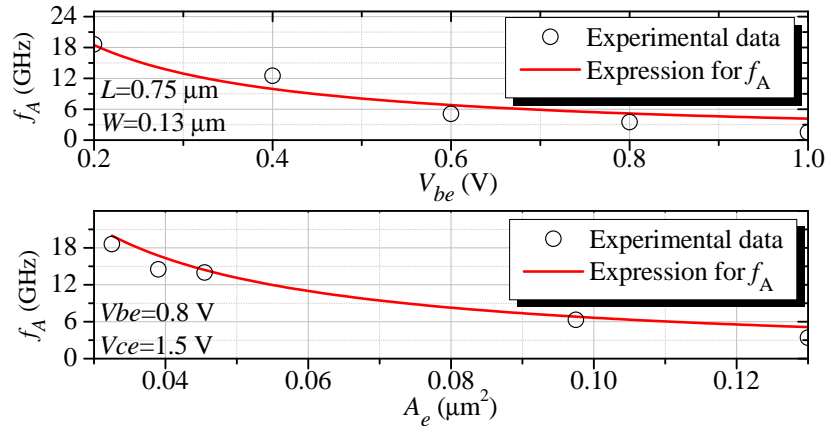


**Figure 4.16:** Experimentally obtained and modeled  $f_A$  showing its dependence with geometry and applied bias.

---

## 4.4 Conclusions and Original Contributions

A methodology to determine the parasitic influence of the substrate in SiGe HBTs has been proposed, evidencing the errors in the modeling when ignoring the bias dependence of the associated elements. This methodology allows modeling CE and CB-configured SiGe HBTs in a consistent and physically based fashion. Excellent model–experiment correlations are obtained for devices operating in the active region up to 60 GHz, which is fundamental to identify the optimal configuration for power amplification at a given frequency. In this regard, a simple and analytical expression was also proposed for the calculation of the frequency at which the CE and CB MAG curves crossover.

## General Conclusions

THE implementation and improvement of compact and equivalent circuit models to perform reliable microwave circuit-oriented simulations on advanced BiCMOS technologies has been presented throughout this dissertation. An exhaustive study of experimental data corresponding to SiGe HBTs fabricated in advanced  $0.13\ \mu\text{m}$  BiCMOS technologies has been carried out, pointing out the effects that become important when technology evolves. Furthermore, several physically based extraction strategies have been proposed, explaining their corresponding advantages and constraints, evidencing also that a good knowledge of the used test fixture is an essential part in the high-frequency characterization and design of RF integrated systems.

In this chapter, some important conclusions derived from the performed research are presented. The reader will figure out that there is still much work to be done in future research, which is the consequence and reason why the HBT is currently one of the most studied semiconductor devices for high-frequency applications.

## 5.1 Test Fixtures for High-Frequency Characterization

High frequency characterization is an essential part in the design of successful RF integrated systems, and although the VNA is a powerful tool for HF characterization, it can only provide useful measurements between well calibrated reference planes. Thus, a test fixture to connect the calibrated reference plane of the VNA to the DUT is required. These test fixtures alter the measurement results and must be de-embedded for the highest quality of the measurement. This dissertation has shown a physics-based methodology that contributes in the understanding of the origin of the parasitics introduced by the necessary test fixture, which helps to improve the test fixture design for either test planing or prototyping. Also, by knowing the physical origin of the losses introduced by the fixture, de-embedding procedures and RF-measurement techniques can be improved, ensuring the reliable characterization of the DUT.

## 5.2 Parameter Extraction Methodologies

Regarding the parameter extraction methods for advanced bipolar devices, the results show that the proposed methodologies are more accurate and simpler than previously reported approaches, which allows implementing reliable high-frequency HBT models that properly represent the device's input and output electrical characteristics even under different bias conditions. This stands for an important contribution to ease circuit oriented modeling since the proposed methods have been validated using state-of-the-art devices. In addition, since the extraction methods developed in this dissertation are based on device physics, they can be used as a base to design experiments to determine technological parameters such as doping concentrations and effective dimensions. Thus, they can be considered as a guideline for future work.

## 5.3 Compact and Equivalent Circuit Models

Throughout this dissertation, the input and output electrical characteristics of SiGe HBTs were analyzed and modeled by means of compact and equiv-

alent circuit models. Both types of models present several advantages and disadvantages, which suggests that the application requirements determine the model to be used. In this regard, the calculation results based on the simple one-emitter-finger layout showing the distributed nature of HBTs, can be further extended to developing a CAD tool to study a more complicated geometry including arrays of HBTs with multi-finger emitters. Thus, complementing results from thermal modeling, RF-IC designers may have a tool to design HBT layouts with an optimized high frequency performance. This compact model helps to develop an equivalent circuit model easy to implement in conventional circuit simulators, such as SPICE, in which the high frequency distributed effect of voltage and current in the intrinsic and polysilicon base region has been included, demonstrating that the complex base impedance impacts the power gain of the transistor, especially for CB configured HBTs. Moreover, this dissertation provides an analytical expression to determine the frequency where the power gain of an HBT configured in CE and CB configurations crossover, which can guide the HBT IC design and the selection of operation configurations. Thus, specific operation frequency ranges have been given for guiding the selection of operation configuration, providing valuable design guidelines for RF-ICs based on SiGe HBTs.

## 5.4 Emerging Modeling Topics

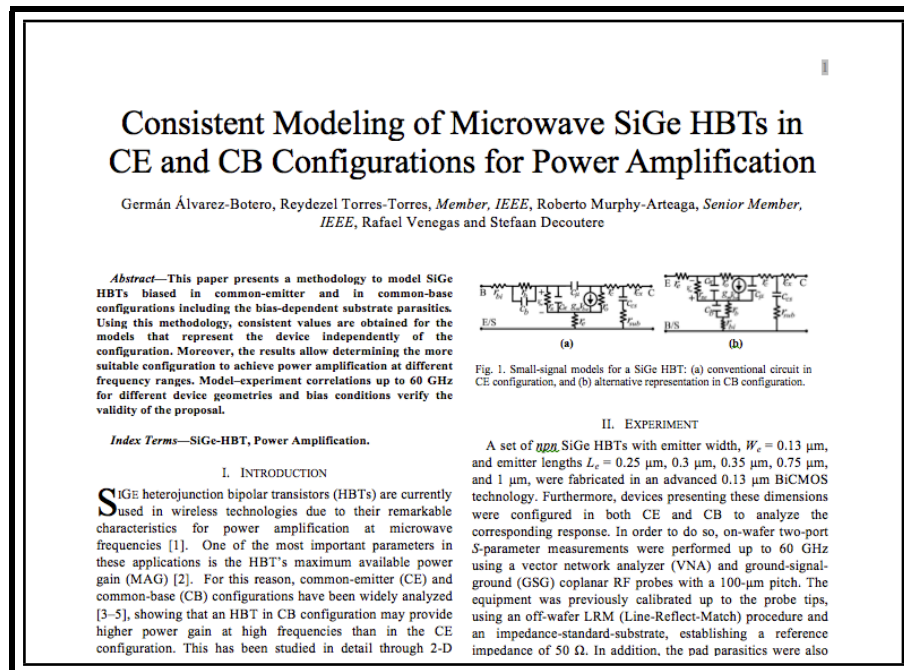
The continuous evolution of modern technologies and the rising demand of high speed devices has accentuated the influence of some effects that have been previously neglected. For instance, the scaling down of new generations of BiCMOS technologies has brought that the parasitic extrinsic effects surrounding the HBT are becoming much larger than its intrinsic characteristics, thus, new accurate techniques to de-embed them in order to accurately model advanced devices will have to be proposed.

Also, the inductive effects at the HBT's terminals may become important as technology evolves due to the combined impact of the distributed effects at the base and the relatively long strips used to interconnect the devices.

Finally, it is important to remark that in this dissertation, only the electrical characteristics of the HBT has been modeled. Therefore, the electro-thermal modeling of the device emerges as a topic derived from this dissertation.

## Publications Derived from this Dissertation

- G. Álvarez-Botero, R. Torres-Torres, R. Murphy-Arteaga, R. Venegas and S. Decoutere “*Consistent Modeling of Microwave SiGe HBTs in CE and CB Configurations for Power Amplification*”, submitted to IEEE Microwave and Wireless Components Letters, 2013.



- **G. Álvarez-Botero**, R. Torres-Torres, and R. Murphy-Arteaga, “Modeling the Distributed Physical Effects in the Intrinsic Base of SiGe HBTs Using Transmission Line Concepts”, in Proceedings of the International Conference on Simulation of Semiconductor Processes and Devices (SISPAD), 2012, pp. 320–323.

SISPAD 2012, September 5-7, 2012, Denver, CO, USA

## Modeling the Distributed Physical Effects in the Intrinsic Base of SiGe HBTs Using Transmission Line Concepts

Germán Álvarez-Botero, Reydezel Torres-Torres and Roberto Murphy-Arteaga  
*galvarez@inaoep.mx, reydezel@inaoep.mx, rmurphy@inaoep.mx*  
 National Institute for Astrophysics, Optics and Electronics (INAOE)  
 Department of Electronics  
 Tonantzintla, Puebla, Mexico

**Abstract**—The applicability of a transmission line model for representing the distributed high frequency effects in a SiGe HBT is demonstrated in this paper. In addition, the corresponding parameter extraction from S-parameter measurements is proposed, allowing to achieve excellent model-experiment correlation of the electrical behavior of the device's input characteristics up to 60 GHz.

**Index Terms**—Heterojunction Bipolar Transistor, Distributed model, Parameter Extraction.

### I. INTRODUCTION

SiGe BiCMOS technology provides an attractive solution to address the exigencies in performance of microwave integrated circuits for modern communication systems [1], [2]. In fact, recent papers predict that in the near future HBTs will be operating beyond the microwave frequency range [3]. However, even though there are recent papers dealing with the modeling of these devices up to some tens of gigahertz [4], [5], the corresponding accuracy is limited since the available models ignore the distributed nature of the structure of an HBT. This paper demonstrates that applying a rigorous Transmission Line analysis to the effects occurring in SiGe HBTs allows for a proper representation and physical model parameter extraction up to 60 GHz in a simple and straightforward way.

### II. EXPERIMENT

In order develop and verify the validity of the model proposed in this work, common-emitter SiGe HBTs were fabricated on p-type Si substrate in a  $0.13\ \mu\text{m}$  BiCMOS technology. Afterwards, on-wafer two-port measurements up to 60 GHz were taken on these devices using a vector network analyzer (VNA) and ground-signal-ground (GSG) coplanar RF probes with a  $100\ \mu\text{m}$  pitch. In this work, the HBTs were biased at  $V_E = V_C = 0\ \text{V}$  in order to analyze the parasitics associated with the base-to-emitter junction. This particular bias is selected since the effect of the collector current is negligible in the small-signal model when the device is operating under this condition. The VNA was previously calibrated up to the probe tips, as shown in Fig. 1, using an off-wafer LRM

(line-reflect-match) procedure, and an impedance-standard-substrate, establishing by this way a reference impedance of  $50\ \Omega$ .

Notice also in Fig. 1 that the DUT is embedded between pads and other interconnects to allow for the corresponding probing. In order to minimize the undesired effects associated with these interconnects, the pads are isolated from the substrate by using metal ground shields to reduce the coupling of the pads through the substrate. Nonetheless, the pad parasitic effects were also deembedded from the measurements by applying a two-step procedure and measurements collected from an 'open' and a 'short' dummy structures [6].

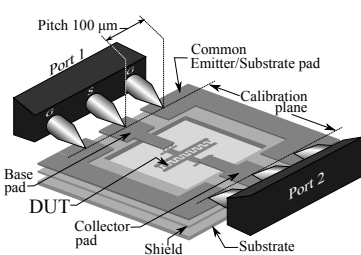


Fig. 1. Test structure pad configuration.

### III. THEORY

Fig. 2 shows a simplified sketch illustrating how the HBT structure is represented using a distributed network, which considers the capacitances associated with the space charge layer at each side of the base region. These capacitances are referred to as base-emitter ( $C_{be}$ ), and base-collector ( $C_{bc}$ ) junction capacitances per unit length; the corresponding value depends on the doping profile and on the width of the associated depletion region.  $r_{bi}$  is the intrinsic base resistance, which is a function of the bias conditions since the width of the space

SISPAD 2012 - <http://www.sispad.org>

320

- G. Álvarez-Botero, R. Murphy-Arteaga, and R. Torres-Torres, “Accurate Modeling to Characterize the Distributed Substrate Effects in SiGe HBTs”, in Proceedings of the XVIII International Iberchip Workshop, 2012, pp. 151–154.

Proceedings of the XVIII International IBERCHIP Workshop

## Accurate Modeling to Characterize the Distributed Substrate Effects in SiGe HBTs

Germán Álvarez-Botero<sup>\*</sup>, Roberto Murphy-Arteaga<sup>†</sup> and Reydezel Torres-Torres<sup>§</sup>  
<sup>\*</sup>galvarez@inaoep.mx, <sup>†</sup>rmurphy@inaoep.mx, <sup>§</sup>reydezel@inaoep.mx  
 Instituto Nacional de Astrofísica, Óptica y Electrónica (INAOE)  
 Department of Electronics  
 Tonantzintla, Puebla, Mexico

**Abstract**—The applicability of a distributed RC model for representing the substrate parasitic effects in a SiGe HBT is demonstrated in this paper. In addition, the corresponding parameter extraction from S-parameter measurements is proposed, allowing to achieve excellent model-experiment correlation of the electrical behavior of the device's output characteristics up to 40 GHz.

**Index Terms**—Heterojunction Bipolar Transistor, Distributed model, Parameter Extraction.

### I. INTRODUCTION

The requirements of modern communication systems put stringent demands on semiconductor technologies for providing performance at a low cost [1]. BiCMOS technology based on SiGe heterojunction bipolar transistors (HBTs) provides an attractive solution to address these exigencies, due to the inherent properties of the SiGe HBTs, such as low noise, high linearity, and low power consumption. However, these remarkable characteristics can be considerably degraded in the microwave range due to the influence of the substrate parasitic effects, which become more important as the operation frequency rises. For this reason, for advanced RF circuit design, the impact of the substrate effects must be correctly accounted for in the modeling of the HBTs.

For an adequate modeling of the substrate effects, it is necessary developing physically based models according to the device structure. For instance, in the present analysis it is important considering the buried layer ( $n^+$ ) (referred to in subsequent as the sub-collector), the depletion region of the sub-collector-substrate junction, the resistive nature of the bulk substrate ( $p^-$ ), and the channel stopper ( $p$ ). A cross-section of the HBT under study showing this structure is presented in Fig. 1.

Fig. 1. Sketch of a HBT cross section showing its physical structure.

Usually, a lumped RC equivalent circuit model is used to represent the substrate characteristics. This is shown at the bottom of Fig. 2, which considers the depletion capacitance formed at the bottom of the sub-collector-substrate junction by means of  $C_{sub}$ . Connected in series to this capacitance, the influence of the inner substrate resistance, and the additional associated with the channel stopper and the substrate contact resistance are taken into account by  $R_{sub}$ . This lumped approach is widely used; however, it is restricted for application at relatively low frequencies since when the frequency increases it is not accurate enough, yielding errors when representing the output impedance of the transistor and the actual gain [2].

Fig. 2. Sketch of a HBT cross section and its corresponding equivalent circuit model considering a lumped model for the substrate network.

The frequency limitations of the typical HBT model are associated to the fact that it neglects the peripheral capacitance of the sub-collector-substrate junction and the resistive behavior of the bulk substrate, resulting in significant errors at high frequencies.

Bearing in mind the previously exposed arguments, in this paper a physically-oriented model for represent the substrate electrical characteristics, taking into account the distributed effects of a HBT is proposed. In addition, the corresponding parameter extraction methodology is developed, obtaining a significant improvement on the output characteristics of a HBT in up to 40 GHz.

Playa del Carmen, Mexico, February 29-March 2, 2012

151

ISSN 977-2177-128009



- **G. Álvarez-Botero**, R. Torres-Torres, and R. S. Murphy-Arteaga, “Modeling and parameter extraction of test fixtures for MOSFET on-wafer measurements up to 60 GHz” *International Journal of RF and Microwave Computer-Aided Engineering*, Nov. 2012.

### Modeling and Parameter Extraction of Test Fixtures for MOSFET On-Wafer Measurements up to 60 GHz

Germán Álvarez-Botero, Reydezel Torres-Torres, Roberto S. Murphy-Arteaga

Department of Electronics, Instituto Nacional de Astrofísica, Óptica y Electrónica, INAOE, 72840, Puebla, Mexico

Received 19 July 2012; accepted 1 October 2012

**ABSTRACT:** We present a circuit model and parameter determination methodology for test fixtures used for on-wafer S-parameter measurements on CMOS devices. The model incorporates the frequency dependence of the series resistances and inductances due to the skin effect occurring in the metal pads. Physically based representations for this effect allow for excellent theory-experiment correlations for different dummy structures, as well as when de-embedding transistor measurements up to 60 GHz. © 2012 Wiley Periodicals, Inc. *Int J RF and Microwave CAE* 00:000–000, 2012.

**Keywords:** RF-measurements; S-parameters; test fixtures; equivalent circuit modeling; CMOS devices

#### 1. INTRODUCTION

The characterization and modeling of microwave devices require high-frequency on-wafer measurements. In this case, to make a connection with the probe tips and to apply the RF stimulus to the device under test (DUT), a test fixture is necessary. This introduces considerable parasitic effects between the calibrated reference plane and the DUT, which have a high impact on the quality of the RF measurements. Generally, the parasitic effects of the test fixture are removed from the experimental data using a de-embedding procedure. This is based on the separate measurement of a set of dummy structures (e.g., open, short and through dummies) and then removing the corresponding effects from a complete structure, that is, including the DUT [1–3]. Therefore, the efficiency of these methods is linked to the quality of test fixtures used for the characterization of microwave devices [4].

Additionally, it is important to mention that when measuring dummy structures (e.g., open circuited dummies), substantial noise may be present at high frequencies as measurement uncertainty increases as the impedance of the measured structure becomes higher [5, 6]. Thus, understanding the physical origin of the parasitics for a more complete knowledge of the influence of the test structures on the measurements is needed. This is

especially important to define the frequency range up to where the test fixture is practical, to optimize the layout design of the pads, and to evaluate the sensitivity of specific DUT model parameters to a particular de-embedding method.

Approaches such as modeling the probe pads, interconnections, and DUT in a cascade configuration have been proposed, and these aim at identifying and removing the parasitic effects from raw measurements [7]. However, the origin of the parasitics or their relation to the embedding network layout is not possible using these techniques. The relation with the physical structure is more evident when the unwanted effects of the test fixtures are modeled separating their influence in impedance ( $Z$ ) and admittance ( $Y$ ) blocks, a methodology which in turn has allowed for a deeper understanding of these high frequency effects through the development of equivalent circuit models [8, 9].

Nevertheless, most of these models consist of frequency independent circuit elements, and the modeling of crucial high frequency effects, such as the skin effect, which significantly affects the series resistive and inductive elements in the models for on-wafer pad structures, tend to produce very large ladder circuits [10], increasing the complexity of the extraction methodologies.

To overcome these limitations, this article presents how the skin effect can be satisfactorily incorporated into the modeling of test fixtures in an RF-CMOS process, showing the convenience of including this important high frequency effect. A simple extraction methodology based on transmission-line concepts was developed, and the

Correspondence to: G. Álvarez-Botero; e-mail: galvarez@inaoep.mx  
DOI 10.1002/mmce.20701  
Published online in Wiley Online Library  
(wileyonlinelibrary.com).

© 2012 Wiley Periodicals, Inc.

- G. Álvarez-Botero, R. Murphy-Arteaga, and R. Torres-Torres, “Parameter Extraction Method for Modeling SiGe HBTs Using Cold Condition S-parameter Measurements”, in Proceedings of the VXII International Iberchip Workshop, 2011.

## Parameter Extraction Method for modeling SiGe HBTs Using Cold Condition S-parameter Measurements

Germán Álvarez-Botero\*, Roberto Murphy-Arteaga<sup>†</sup> and Reydezel Torres-Torres<sup>§</sup>

\*galvarez@inaoep.mx, <sup>†</sup>rmurphy@inaoep.mx, <sup>§</sup>reydezel@inaoep.mx  
 Instituto Nacional de Astrofísica, Óptica y Electrónica (INAOE)  
 Department of Electronics  
 Tonantzintla, Puebla, Mexico

**Abstract**—In this work a new parameter extraction method based on the S-parameter measurements of HBTs biased in the cold condition is proposed. The extraction technique gives excellent agreement between the equivalent circuit and the measured S-parameters of a SiGe HBT up to 30GHz.

**Index Terms**—Heterojunction Bipolar Transistor, Parameter Extraction

### I. INTRODUCTION

For circuit design to be reliable, it is necessary to translate the physical behavior of transistors to the simulator properly. This need has resulted in different types of models describing the operation of the transistor, including structural physical models, compact models and equivalent circuit models. Hence, accurate parameter extraction of their constituent parameters is crucial for the development of HBT circuits and applications.

In this sense, the present work focuses on the modeling of SiGe heterojunction bipolar transistor from their small-signal description, adopting an equivalent circuit based on the well-known  $\pi$ -topology, which is popular in commercial circuit simulators such as the Vertical Bipolar Inter-Company Model (VBIC), the Most Exquisite Transistor Model (MEXTRAM) or the High Current Model (HICUM) [1]–[3].

We propose a simple parameter extraction method, with which all model parameters are extracted directly from S-parameter measurements of an HBT polarized in the cold condition. This technique is widely used since the resulting equivalent circuit is simpler than the forward mode one [4], allowing the extraction of HBT parameters with great accuracy without previous knowledge of some geometrical or material parameters, for example, methods like [5], [6], require the knowledge or obtention by non-linear iteration of the built-in potentials and grading coefficients of the capacitive junctions, requirements that may be regarded as a limitation in the development of the extraction methodology.

### II. EXPERIMENT

The device under test (DUT) was a common emitter SiGe HBT fabricated on a  $0.13\ \mu\text{m}$  BiCMOS process, biased at  $V_{BE} = 0$  and  $V_{BC} < 0$ . On-wafer two-port S-parameter measurements were performed up to 30 GHz using a vector network analyzer (VNA) and ground-signal-ground (GSG) coplanar RF probes. The equipment was previously calibrated up to the probe tips, as shown in Fig. 1, using an SOLT (Short-Open-Line-Through) procedure. The power applied in each port was  $-20\ \text{dBm}$  which corresponds to  $10\ \mu\text{W}$ .

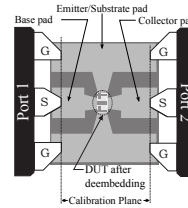


Fig. 1. Test structure pad configuration.

### III. PROPOSED METHOD AND RESULTS

Fig. 2 shows the small-signal equivalent circuit of a SiGe HBT in the forward operation mode; in this,  $R_{be}$ ,  $R_e$  and  $R_{ce}$  are the extrinsic resistances associated with the base, emitter and collector regions;  $C_1$  and  $C_{sub2}$  represent the remaining parasitic capacitances not removed in the deembedding procedure;  $C_{bcx}$  is the extrinsic capacitance associated with the base-collector junction;  $R_{bk}$  and  $C_{bk}$  are the elements associated with the substrate;  $R_{bs}$ ,  $R_{ps}$ ,  $C_{ps}$ ,  $C_{bc}$  and the transconductance  $gm$  are the parameters associated with the intrinsic operation of the transistor.



## Resumen Ejecutivo en Español

CON la conciencia que el conocimiento debe documentarse en un lenguaje común a todos los actores del quehacer científico, esta disertación se ha escrito en su versión en extenso en inglés. Sin embargo, la convicción de dejar en cada paso hacia el conocimiento colectivo una memoria en el idioma propio donde dicho desarrollo ha sido generado ha motivado a presentar una versión resumida en español de esta tesis, que condensa las principales ideas descritas en la misma. Bajo el entendido que no se trata de una traducción del escrito en inglés y por la brevedad de este resumen, muchas ideas no se discuten con profundidad. Así mismo, las ecuaciones, figuras y tablas mencionadas corresponden a las presentadas en el texto en inglés, con la finalidad de evitar la duplicación de las mismas.

### Capítulo 1. Introducción general.

Desde su invención a finales de años 40, el transistor ha sido un dispositivo crucial para el desarrollo de la electrónica moderna, siendo parte actualmente de una amplia gama de aplicaciones. Sin embargo, a pesar de los avances en los procesos de fabricación de los transistores modernos, éstos trabajan bajo los mismos principios básicos que el transistor bipolar patentado por Bardeen, Brattain y Shockley. Una replica de éste se muestra en la Fig. 1.

Esas similitudes conceptuales entre los primeros transistores y los empleados en la actualidad, ha contribuido a que muchos de los modelos teóricos formulados originalmente continúen siendo utilizados para representar los dispositivos actuales. Así pues, es necesario re-evaluar y actualizar muchos conceptos en concordancia con el desarrollo de las tecnologías modernas que demandan el diseño confiable de nuevas aplicaciones. En particular, la creciente expansión de los sistemas de comunicaciones de alta velocidad han hecho que los transistores bipolares de heterounión (HBTs, por sus siglas en inglés), sean utilizados en una gran gama de aplicaciones en el campo de las microondas, especialmente los basados en SiGe, debido a su excepcional compatibilidad con los procesos estándar de fabricación de circuitos integrados.

Una de las técnicas más utilizadas para caracterizar y modelar las características eléctricas de este tipo de dispositivos, se basa en la medición de parámetros de dispersión (parámetros S). Esta disertación presenta un estudio exhaustivo de las dos alternativas más ampliamente utilizadas para modelar transistores bipolares avanzados en el rango de operación de las microondas: el modelado compacto y con circuitos equivalentes. Ambas propuestas son implementadas a partir de la obtención experimental de parámetros S, proponiendo nuevas metodologías de extracción de los parámetros asociados con cada modelo que representa el funcionamiento del dispositivo. Dichas metodologías muestran mejoras notables con respecto a las existentes en la literatura, ya que permiten representar el comportamiento eléctrico los dispositivos en altas frecuencias de manera confiable, conservando el significado físico de los parámetros que constituyen cada modelo.

## **Capítulo 2. Modelado de las estructuras de prueba utilizadas para la caracterización de dispositivos de microondas BiCMOS.**

La caracterización de dispositivos requiere de estructuras que permitan la conexión entre las puntas de prueba y el dispositivo bajo estudio (DUT, por sus siglas en inglés). Estas estructuras introducen considerables efectos parásitos, los cuales deben ser adecuadamente removidos, con la finalidad de obtener una representación confiable de las características eléctricas propias del DUT. Estos efectos parásitos se acentúan a medida que la frecuencia, a la

cual es necesario caracterizar los dispositivos se incrementa. Por lo tanto, entender su origen físico permite mejorar los procedimientos de caracterización, las técnicas de des-incrustamiento, y el modelado propio de los dispositivos, a través de la optimización en el diseño de las estructuras de prueba.

Habitualmente, para remover los efectos parásitos introducidos por las estructuras de prueba, se emplean procedimientos basados en estándares, que no consideran la relación entre la arquitectura física de la estructura de prueba, y el origen de los efectos indeseados introducidos por la misma. Así, utilizando una representación mediante un modelo de circuito equivalente, se determinó la dependencia con la frecuencia de cada uno de sus elementos constitutivos, en este caso se utilizó un modelo compuesto por *RLGC*, distribuidos como se muestra en la Fig. 2.4. El valor de cada parámetro en general depende de factores geométricos así como de los materiales utilizados. Sin embargo, los elementos en serie, denominados como  $Z_i$  en la Fig. 2.4, presentan una importante dependencia con la frecuencia, esto debido al confinamiento de la corriente en la superficie del metal, debido al efecto piel. Este efecto comienza a ser notable para la estructura de prueba estudiada a partir de 14 GHz, como se muestra en la Fig. 2.6. Este efecto es consistentemente descrito mediante las ecuaciones (2.8) y (2.9), como se muestra en la Fig. 2.5. El modelo propuesto, una vez obtenidos todos sus parámetros constitutivos mediante la metodología presentada en esta disertación, describe adecuadamente los resultados experimentales, y evidencia la necesidad de incluir los efectos propios de incrementar la frecuencia en el modelado de las estructuras de prueba, como se ilustra en las Figuras 2.8 y 2.9. El impacto al remover estos efectos parásitos de los datos experimentales obtenidos al medir un HBT polarizado en la región activa, sin considerar cómo la estructura de pruebas es influenciada por efectos de alta frecuencia, se muestra en la Fig. 2.10, evidenciando los posibles errores en los cuales se puede incurrir en el modelado de dispositivos, a medida que mayores frecuencias de operación son requeridas.

## Capítulo 3. Modelado de los efectos distribuidos en SiGe HBT.

Los modelos mas comunes para representar la operación del HBT utilizan una aproximación cuasi-estática (QS, por sus siglas en inglés), esto es, que suponen que los electrones y huecos se mueven con velocidad infinita, por lo tanto, al aplicar un estímulo externo, la respuesta en los terminales del transistor es inmediata. Sin embargo, a medida que la frecuencia de operación se incrementa, es más evidente que los dispositivos no pueden responder de forma inmediata ante un estímulo. Una forma de representar este escenario, es mediante la utilización de un modelo distribuido. Con el desarrollo de esta tesis se ha mostrado que este tipo de efectos, denominados efectos no-cuasi-estáticos (NQS, por sus siglas en inglés), afectan, para un dispositivo configurado en emisor común, tanto el puerto de entrada (a través de la terminal de base), como el puerto de salida (a través de la terminal de colector). Así, en esta disertación se han propuesto, a partir de la solución de las ecuaciones del telegrafista (ecuaciones 3.7 y 3.8), un modelo híbrido basado en los conceptos básicos de líneas de transmisión, que permite representar los efectos distribuidos en la región de base, y que afectan la impedancia de entrada; así como aquellos que afectan la impedancia de salida, debido a las pérdidas asociadas al sustrato. Las metodologías necesarias para obtener los parámetros constitutivos de dicho modelo, también son propuestos como parte de este trabajo. Como se puede apreciar en las Figuras 3.11, 3.16 y 3.17, se obtiene una excelente correlación entre la simulación correspondiente a los modelos propuestos en esta tesis, y los datos experimentales medidos hasta 60 GHz, validando de esta forma que tanto la impedancia del puerto de entrada, como del puerto de salida, deben considerar la naturaleza distribuida del HBT a medida que se incrementa la frecuencia de operación.

## Capítulo 4. Modelado de SiGe HBTs configurados en CE y CB para amplificación de potencia.

Cuando se diseñan amplificadores que operan en el rango de las microondas utilizando HBTs, es posible optimizar su desempeño utilizando diferentes etapas de amplificación, con transistores en diferentes configuraciones. Con la motivación de desarrollar un modelo consistente en las configuraciones más

usuales, un conjunto de transistores, configurados tanto en emisor-común (CE, por sus siglas en inglés), como en base-común (CB, por sus siglas en inglés), con anchos de emisor de  $W_e = 0.13 \mu\text{m}$ , y longitudes de emisor de  $L_e = 0.25 \mu\text{m}$ ,  $0.3 \mu\text{m}$ ,  $0.35 \mu\text{m}$ ,  $0.75 \mu\text{m}$ , y  $1 \mu\text{m}$ , fueron estudiados bajo diferentes condiciones de polarización.

La dependencia de la capacitancia asociada a la unión colector-substrato, la cual usualmente es determinada cuando  $V_{be} = 0 \text{ V}$ , y  $V_{ce} = 0 \text{ V}$ , condición conocida como de polarización en frío, fue determinada como función del voltaje de colector aplicado, como se muestra en la Fig. 4.5. Esto evidencia que, para remover adecuadamente el efecto parásito del substrato, con la finalidad de modelar el comportamiento intrínseco del transistor, se debe determinar su efecto en el punto de polarización donde el HBT opera, en caso contrario, esto podría ocasionar errores importantes la representación del comportamiento del dispositivo.

A partir del modelo de circuito equivalente presentado en la Fig. 4.6, donde se han removido adecuadamente los efectos parásitos asociados al substrato, se desarrolló una metodología de extracción que permitió obtener los parámetros constitutivos de dicho modelo, cuyos valores obtenidos se condensan en la Tabla 4.1. Utilizando estos valores se realizaron simulaciones de parámetros S, con el transistor operando tanto en configuración de CE, como de CB. Los resultados obtenidos fueron utilizados en conjunto con las ecuaciones (4.14) y (4.15), para obtener la máxima ganancia de potencia que el HBT podría entregar a una carga, conocida como máxima ganancia de potencia disponible (MAG, por sus siglas en inglés). Como se puede observar en la Fig. 4.14, se obtienen excelentes resultados al correlacionar los datos experimentales y los datos obtenidos de la simulación empleando el modelo propuesto. La Fig. 4.14, también presenta los errores en los cuales se puede incurrir al ignorar la dependencia con el voltaje de colector, de los elementos que modelan el comportamiento de la unión colector-substrato. Adicionalmente, esta figura también presenta la fuerte dependencia que tienen los dispositivos estudiados con la naturaleza compleja de la región de base, representada por  $Z_b$ . Este comportamiento es usualmente ignorado en los modelos convencionales, pero cobra importancia con el aumento de la frecuencia, por lo cual fue incluido, satisfactoriamente, en el presente trabajo de investigación.

Para dar completez al presente estudio, se analizó una de las características más interesantes, comparativamente hablando, de los transistores bipolares configurados en CE y CB, esto es, que a medida que la frecuencia se incrementa, los transistores configurados en CB presentan mejores características como amplificadores de potencia, que aquellos configurados en CE. Por lo tanto, en este trabajo se propone una expresión para determinar analíticamente el rango de frecuencia donde un HBT presenta mejores características como amplificador de potencia, de acuerdo con la configuración utilizada. La expresión (4.22), representa la frecuencia a partir de la cual un transistor configurado en CB, comienza a presentar una mayor ganancia de potencia, que uno configurado en CE. Este resultado es una expresión de gran utilidad para el diseño de amplificadores que operan en el rango de las microondas utilizando HBTs.

## Capítulo 5. Conclusiones Generales.

En esta disertación se ha presentado la implementación de modelos compactos y de circuito equivalente para la simulación en altas frecuencias de HBTs fabricados en tecnologías avanzadas BiCMOS. Por esta razón, se ha llevado a cabo un estudio detallado de datos experimentales que ha permitido identificar los efectos que adquieren importancia a medida que la tecnología evoluciona. Se han prestado especial atención a las características experimentales y a la obtención de modelos adecuados que permitan identificar y remover adecuadamente los efectos parásitos asociados a las estructuras de prueba, contribuyendo a la comprensión de su origen físico y su impacto a medida que se expanden los rangos de aplicación en frecuencia. Así, con respecto a la extracción de parámetros, este trabajo presenta métodos confiables para la determinación de los elementos parásitos introducidos en el proceso de caracterización, llevando a la caracterización confiable de los dispositivos.

Se han presentado, tanto modelos compactos que representan el comportamiento en altas frecuencias de los HBTs, incluyendo efectos NQS, de gran utilidad en simuladores de dispositivos, como modelos de circuito equivalente, cuya implementación en simuladores de circuitos permitirá el diseño confiable de nuevas aplicaciones en el rango de las microondas. Por otra parte, se desarrollaron modelos mejorados para la representación apropiada



del HBT de acuerdo con su configuración, haciendo un detallado análisis de la ganancia de potencia tanto en emisor como en base común y definiendo el rango en el cual cada configuración presenta sus mejores características como amplificador de potencia.

También es necesario mencionar la necesidad de realizar investigación concerniente al modelado de dispositivos avanzados, ya que la evolución de la tecnología, la reducción en las dimensiones de los dispositivos, la inclusión de nuevos materiales, y la demanda de mayores frecuencias de operación, introduce efectos despreciados en los modelos convencionalmente usados en el diseño de circuitos de RF. Adicionalmente, se debe remarcar la necesidad de considerar al HBT como un dispositivo de cuatro terminales, lo cual es aún un tema abierto de investigación.

## List of Figures

1.1	A replica of the first working transistor, AT&T labs, 1948. . .	1
1.2	RF application spectrum overlaid with technology performance [10].	3
1.3	DUT configured as a two-port network showing the S-parameter definitions. . . . .	4
1.4	Measurement setup for on-wafer S-parameters. . . . .	5
1.5	Test structure for performing S-parameter measurements showing the pad configuration for probing. . . . .	6
1.6	Small-signal model of an HBT illustrating its extrinsic elements.	8
1.7	Intrinsic topologies (a) $\pi - g_m$ , (b) $\pi - \beta$ and (c) T- $\alpha$ of an HBT. . . . .	9
1.8	Simple feedback networks that would be used together with $\pi - g_m$ , $\pi - \beta$ or T- $\alpha$ topologies. . . . .	9
2.1	Cross sectional view showing the distribution of the electric field in: through the substrate (a) a conventional test fixture and, (b) a shielded test fixture. . . . .	14
2.2	(a) Sketch of a DUT embedded in a test fixture, (b) corresponding equivalent circuit model consisting of generic impedance and admittance blocks, and (c) associated dummy structures for de-embedding. . . . .	14
2.3	Equivalent circuit models for the dummy structures. . . . .	15

2.4	Equivalent circuit model for the test fixture using $RLGC$ elements. . . . .	17
2.5	Linear regressions used to determine $R_{LFi}$ , $K_i$ , and $L_{HFi}$ . . . . .	18
2.6	Skin depth calculated for aluminum, which is the metal used to form the probing pads used in this project. . . . .	19
2.7	Linear regressions used to determine (a) $L_s$ , (b) $C_i$ , and (c) $C_1$ . . . . .	20
2.8	Comparison between simulated and experimental data corresponding to the Open structure when using the models that consider $f$ -independent (FIM) and $f$ -dependent (FDM) series elements. . . . .	21
2.9	Comparison between simulated and experimental data corresponding to the Short structure when using the models that consider $f$ -independent (FIM) and $f$ -dependent (FDM) series elements. . . . .	22
2.10	S-parameters for a de-embedded SiGe HBT under $V_{be} = 0.8$ V and $V_{ce} = 2$ V bias condition. . . . .	24
3.1	Sketch of an HBT cross section showing the currents influenced by the NQS effects. . . . .	27
3.2	Cross section of an HBT showing the small-signal distributed equivalent circuit model. . . . .	28
3.3	Sketch of an HBT cross section showing the SGP representation for the substrate parasitics. . . . .	29
3.4	Sketch of an HBT cross section and its corresponding equivalent circuit model considering an RC-lumped model for the substrate network. . . . .	29
3.5	Micrograph showing the pad configuration of the HBT, illustrating the experimental array for RF characterization under the cold condition. . . . .	30
3.6	Small-signal equivalent circuit model for a SiGe HBT biased at $V_{BE} = V_{BC} = 0$ . . . . .	31
3.7	Simplified HBT model in common emitter configuration used to derive the proposed substrate model. . . . .	31
3.8	Linear regressions used to determine $C_{be}$ and $C_{bc}$ . . . . .	32
3.9	Sketch of an HBT cross section and its corresponding equivalent circuit considering a distributed model for the substrate network. . . . .	33

3.10	Frequency dependence of the substrate parasitics for a SiGe HBT under $V_{BE} = V_{BC} = 0$ bias condition. . . . .	34
3.11	Comparison between experimental and simulated data for the $S_{22}$ -parameter using a lumped and a distributed network to model the substrate parasitics in a SiGe HBT. . . . .	35
3.12	Micrograph showing the pad configuration of the HBT, illustrating the experimental array for RF characterization under $V_{be} > 0$ V. . . . .	36
3.13	Simplified models: (a) assuming common emitter/substrate configuration at $V_C = 0$ V, and (b) assuming that the HBT is terminated in a short-circuit. . . . .	37
3.14	Linear regression used to determine $g$ and $c$ . . . . .	39
3.15	Linear regression used to determine $r_{bi}$ . . . . .	40
3.16	Simulation-experiment correlation for the real part of $Z_{11}$ . . . . .	41
3.17	Simulation-experiment correlation for the imaginary part of $Z_{11}$ . . . . .	41
4.1	Small-signal equivalent circuit model for a CE SiGe HBT. . . . .	44
4.2	Linear regression used to determine $C_{CS}$ and $r_{sub}$ . . . . .	45
4.3	Cross-sectional view an HBT illustrating the substrate resistance components. . . . .	46
4.4	Bias dependence of $r_{sub}$ . . . . .	46
4.5	Extracted $C_{CS}$ as a function of the applied collector voltage. . . . .	47
4.6	Small-signal equivalent circuit model for a CE SiGe HBT biased at $V_{BE} > 0$ and $V_{CE} = 2$ V. . . . .	47
4.7	Linear regression used to determine $r_c$ and $C_\mu$ . . . . .	48
4.8	Linear regression used to determine $r_b, C_b$ and $r_{bi}$ . . . . .	49
4.9	Linear regression, based on equation 4.10. . . . .	50
4.10	Linear regression, based on equation 4.11. . . . .	50
4.11	Modified Hybrid- $\pi$ model for CE SiGe HBT. . . . .	52
4.12	Equivalent model for (a) CE (b) CB. . . . .	52
4.13	Extracted $C_b$ as a function of the applied voltage. . . . .	53
4.14	Experimental and simulated MAG for CE and CB-configured SiGe HBTs showing the effect of neglecting $C_b$ and the bias dependence of $C_{CS}$ . . . . .	54
4.15	Experimental and simulated power gain curves showing $f_A \approx 2.5$ GHz and $f_{max} \approx 24$ GHz. . . . .	55
4.16	Experimentally obtained and modeled $f_A$ showing its dependence with geometry and applied bias. . . . .	56

## References

- [1] M. Riordan and L. Hoddeson, “Birth of an era,” *Scientific American*, no. December 1947, pp. 10–15, 1997.
- [2] T. H. Ning, “History and Future Perspective of the Modern Silicon Bipolar Transistor,” *IEEE Transactions on Electron Devices*, vol. 48, no. 11, pp. 2485–2491, 2001.
- [3] W. Shockley, “Circuit Element Utilizing Semiconductive Material,” 1951.
- [4] ———, “The Path to the Conception of the Junction Transistor,” *IEEE Transactions on Electron Devices*, vol. ED31, no. 11, pp. 1523–1546, 1984.
- [5] ———, “The Theory of p-n Junctions in Semiconductors and p-n Junction Transistors,” *Bell System Technical Journal*, vol. XXVIII, pp. 435–489, 1949.
- [6] R. P. Jindal, “From Millibits to Terabits per second and Beyond ,À Over 60 years of Innovation,” in *2nd International Workshop on Electron Devices and Semiconductor Technology*, 2009, pp. 1–6.
- [7] J. Bardeen and W. Brattain, “The Transistor, A Semiconductor Triode,” *Proceedings of the IEEE*, vol. 86, no. 1, pp. 29–30, Jan. 1998.

- 
- [8] P. K. Bondyopadhyay, “In the Beginning,” *Proceedings of the IEEE*, vol. 86, no. 1, pp. 63–77, 1998.
- [9] J. Dunn, D. Harame, A. Joseph, S. St. Onge, N. Feilchenfeld, L. Lanzarotti, B. Orner, E. Gebreselasie, J. Johnson, D. Coolbaugh, R. Rassel, and M. Khater, “SiGe BiCMOS Trends-Today and Tomorrow,” in *IEEE Custom Integrated Circuits Conference 2006*. Ieee, Sep. 2006, pp. 695–702.
- [10] ITRS, “International Technology Roadmap for Semiconductors,” Tech. Rep., 2012.
- [11] M. Schroter, “HICUM - A scalable physics-based compact bipolar transistor model,” Tech. Rep., 2000.
- [12] H. C. D. Graaff, W. J. Kloosterman, J. Geelen, and M. Koolen, “Experience With the New Compact MEXTRAM Model for Bipolar Transistors,” in *Proceedings of the 1989 Bipolar Circuits and Technology Meeting*, no. 3, 1989, pp. 3–6.
- [13] G. Gildenblat, Ed., *Compact Modeling*, 1st ed. Springer, 2010.
- [14] H. de Graaff and F. M. Klaassen, “Compact Transistor Modeling for Circuit Design,” 1990.
- [15] M. Schroter and A. Chakravorty, *Compact Hierarchical Bipolar Transistor Modeling With HICUM*. World Scientific Publishing Co., 2010.
- [16] D. M. Pozar, *Microwave Engineering*, 3rd ed. Jhon Wiley & Sons, 2005.
- [17] G. Gonzalez, *Microwave Transistor Amplifiers*, 2nd ed. Prentice-Hall, 1997.
- [18] M. Rudolph, R. Doerner, K. Beilenhoff, and P. Heymann, “Scalable GaInP/GaAs HBT large-signal model,” *IEEE Transactions on Microwave Theory and Techniques*, vol. 48, no. 12, pp. 2370–2376, 2000.
- [19] P. J. Tasker and M. Fernández-Barciela, “HBT small signal T and  $\pi$  model extraction using a simple, robust and fully analytical procedure,” in *Proceedings of the 2002 IEEE MTT-S International Microwave Symposium Digest.*, 2002, pp. 2129–2132.

- [20] D. A. Teeter and W. R. Curtice, "Comparison of Hybrid Pi and Tee HBT Circuit Topologies and Their Relationship to Large Signal Modeling," in *IEEE MTT-S International Microwave Symposium Digest*, vol. 3, 1997, pp. 375–378.
- [21] T.-R. Yang, J. M.-L. Tsai, C.-L. Ho, and R. Hu, "SiGe HBTs Small-Signal Pi Modeling," *IEEE Transactions on Microwave Theory and Techniques*, vol. 55, no. 7, pp. 1417–1424, Jul. 2007.
- [22] S. Wartenberg, "RF Test Fixture Basics," *Microwave Journal*, no. June, pp. 1–10, 2003.
- [23] R. Hooper, D. Shuffield, K. Merchant, and D. Savage, "Common RF test platform," in *2011 IEEE Autotestcon*. Ieee, Sep. 2011, pp. 40–46.
- [24] X. Ye, "De-embedding errors due to inaccurate test fixture characterization," *IEEE Electromagnetic Compatibility Magazine*, vol. 1, no. 4, pp. 75–78, 2012.
- [25] R. Torres-Torres, R. Murphy-Arteaga, and J. A. Reynoso-Hernández, "Analytical Model and Parameter Extraction to Account for the Pad Parasitics in RF-CMOS," *IEEE Transactions on Electron Devices*, vol. 52, no. 7, pp. 1335–1342, 2005.
- [26] M. Ferndahl, C. Fager, K. Andersson, P. Linnér, H.-O. Vickers, and H. Zirath, "A General Statistical Equivalent-Circuit-Based De-Embedding Procedure for High-Frequency Measurements," *IEEE Transactions on Microwave Theory and Techniques*, vol. 56, no. 12, pp. 2692–2700, 2008.
- [27] E. F. Calandra, "Measurement-Based Modeling of Microwave Transistor Package and Test-Fixture for Device S-Parameter Deembedding," in *Proceedings of the 37th Midwest Symposium on Circuits and Systems*, 1995, pp. 1227–1230.
- [28] M.-H. Cho, G.-W. Huang, C.-S. Chiu, K.-M. Chen, A.-S. Peng, and Y.-M. Teng, "A Cascade Open-Short-Thru (COST) De-Embedding Method for Microwave On-Wafer Characterization and Automatic Measurement," *IEICE Transactions on Electronics*, vol. E-88-C, no. 5, pp. 845–850, 2005.

- [29] H. Cho and D. E. Burk, "A Three-Step Method for the De-Embedding of High-Frequency S-Parameter Measurements," *IEEE Transactions on Electron Devices*, vol. 38, no. 6, pp. 1371–1375, 1991.
- [30] T. Kolding, "A Four-Step Method for De-Embedding Gigahertz On-Wafer CMOS Measurements," *IEEE Transactions on Electron Devices*, vol. 47, no. 4, pp. 734–740, Apr. 2000.
- [31] I. M. Kang, S.-j. Jung, T.-h. Choi, J.-h. Jung, C. Chung, H.-s. Kim, H. Oh, H. W. Lee, G. Jo, Y.-k. Kim, H.-g. Kim, and K.-m. Choi, "Five-Step (Pad-Pad Short-Pad Open-Short-Open) De-Embedding Method and Its Verification," *IEEE Electron Device Letters*, vol. 30, no. 4, pp. 398–400, 2009.
- [32] X. Shi, J.-g. Ma, and K. S. Yeo, "Equivalent Circuit Model of On-Wafer CMOS Interconnects for RFICs," *IEEE Transactions on Very Large Scale Integration (VLSI) Systems*, vol. 13, no. 9, pp. 1060–1071, Sep. 2005.
- [33] S. Mei and Y. Ismail, "Modeling Skin and Proximity Effects With Reduced Realizable RL Circuits," *IEEE Transactions on Very Large Scale Integration (VLSI) Systems*, vol. 12, no. 4, pp. 437–447, Apr. 2004.
- [34] R. Collier and D. Skinner, Eds., *Microwave Measurements*, 3rd ed. IET Electrical Measurement Series, 2007.
- [35] S. H. Hall and H. L. Heck, *Advanced Signal Integrity for High-Speed Digital Designs*, 1st ed. Jhon Wiley & Sons, 2009.
- [36] T. Kolding, "Shield-Based Microwave On-Wafer Device Measurements," *IEEE Transactions on Microwave Theory and Techniques*, vol. 49, no. 6, pp. 1039–1044, Jun. 2001.
- [37] ———, "Shield-Based Microwave On-Wafer Device Measurements," *IEEE Transactions on Microwave Theory and Techniques*, vol. 49, no. 6, pp. 1039–1044, 2001.
- [38] J. Zhang, J. L. Drewniak, D. J. Pommerenke, M. Y. Koledintseva, R. E. Dubroff, W. Cheng, Z. Yang, Q. B. Chen, and A. Orlandi, "Causal RLG(f) Models for Transmission Lines From Measured S-Parameters,"



- IEEE Transactions on Electromagnetic Compatibility*, vol. 52, no. 1, pp. 189–198, 2010.
- [39] A. Schellmanns, J. P. Keradec, and J. L. Schanen, “Electrical Equivalent Circuit for Frequency Dependant Impedance: Minimum Lumped Elements for a Given Precision,” in *Proceedings of the IEEE Industry Applications Conference*, 2000, pp. 3105–3110.
- [40] A. Joseph, J. Dunn, G. Freeman, D. Harame, D. Coolbaugh, R. Groves, K. Stein, R. Volant, S. Subbanna, V. Marangos, S. Onge, E. Eshun, P. Cooper, J. Johnson, J. Rieh, B. Jagannathan, V. Ramachandran, D. Ahlgren, D. Wang, and X. Wang, “Product applications and technology directions with SiGe BiCMOS,” *IEEE Journal of Solid-State Circuits*, vol. 38, no. 9, pp. 1471–1478, Sep. 2003.
- [41] B. Aghdaie and B. Sheu, “Overcoming Limitations of Lumped MOS Models,” *IEEE Circuits and Devices Magazine*, vol. 16, no. 2, pp. 19–26, 2000.
- [42] D. Thomas and J. L. Moll, “Junction Transistor Short-Circuit Current Gain and Phase Determination,” *Proceedings of the IRE*, vol. 40, pp. 1481–1483, 1952.
- [43] M. Rudolph, F. Lenk, R. Doemer, and P. Heymann, “Towards a Unified Method to Implement Transit-Time Effects in Pi-Topology HBT Compact Models,” in *Proceedings of the 2002 IEEE MTT-S International Microwave Symposium Digest.*, 2002, pp. 997–1000.
- [44] J. Jacob, A. DasGupta, and A. Chakravorty, “Physics based modeling of non-quasi-static effects in SiGe-HBTs,” in *2009 2nd International Workshop on Electron Devices and Semiconductor Technology*. Ieee, Jun. 2009, pp. 1–4.
- [45] S. V. Cherepko and J. C. M. Hwang, “Implementation of Nonquasi-Static Effects in Compact Bipolar Transistor Models,” *IEEE Transactions on Microwave Theory and Techniques*, vol. 51, no. 12, pp. 2531–2537, 2003.
- [46] M. Pfof, H.-m. Rein, and T. Holzwarth, “Modeling Substrate Effects in the Design of High-Speed Si-Bipolar IC’s,” *IEEE Journal of Solid-State Circuits*, vol. 31, no. 10, 1996.

- [47] T. K. Johansen, J. Vidkj, V. Krozer, and J. Vidkjaer, "Substrate Effects in SiGe HBT Modeling," in *11th GAAS Symposium.*, Munich, 2003, pp. 445–448.
- [48] T. K. Johansen, V. Krozer, J. Vidkjær, and T. Djurhuus, "Substrate Effects in Wideband SiGe HBT Mixer Circuits," in *13th GAAS Symposium.*, Paris, 2005, pp. 469–472.
- [49] J. Berkner, "Compact Models for Bipolar Transistors," in *Proceedings of the European IC-CAP Device Modeling Workshop*, Berlin, 2002, pp. 1–17.
- [50] R. V. D. Toorn and W. J. Kloosterman, "The Mextram Bipolar Transistor Model," Tech. Rep., 2011.
- [51] S. Fregonese, D. Celi, T. Zimmer, C. Maneux, and P. Sulima, "A Scalable Substrate Network for Compact Modelling of Deep Trench Insulated HBT," *Solid-State Electronics*, vol. 49, no. 10, pp. 1623–1631, Oct. 2005.
- [52] E. Abou-Allam and T. Manku, "An Improved Transmission-Line Model for MOS Transistors," *IEEE Transactions on Circuits and Systems-II*, vol. 46, no. 11, pp. 1380–1387, 1999.
- [53] M. Vaidyanathan and D. L. Pulfrey, "Extrapolated  $f_{max}$  of Heterojunction Bipolar Transistors," *IEEE Transactions on Electron Devices*, vol. 46, no. 2, pp. 301–309, 1999.
- [54] M. Racanelli and P. Kempf, "SiGe BiCMOS Technology for RF Circuit Applications," *IEEE Transactions on Electron Devices*, vol. 52, no. 7, pp. 1259–1270, 2005.
- [55] G. Qin, N. Jiang, G. Wang, and Z. Ma, "Configuration Dependence of SiGe HBT Linearity Characteristics," in *Proceedings of the 1st European Microwave Integrated Circuits Conference*, vol. 7, no. September, 2006, pp. 107–110.
- [56] G. Qin, G. Wang, N. Jiang, and Z. Ma, "Tradeoff between CE and CB SiGe HBTs for Power Amplification in Terms of Frequency-Dependent Linearity and Power-Gain Characteristics," in *Proceedings of the IEEE Topical Meeting on Silicon Monolithic Integrated Circuits in RF Systems*, 2007, pp. 1–4.

- [57] G. Qin, N. Jiang, G. Wang, and Z. Ma, "SiGe HBT linearity comparison between CE and CB configurations," *Semiconductor Science and Technology*, vol. 22, no. 1, pp. S216–S220, Jan. 2007.
- [58] Z. Ma and N. Jiang, "On The Operation Configuration of SiGe HBTs Based on Power Gain Analysis," *IEEE Transactions on Electron Devices*, vol. 52, no. 2, pp. 248–255, Feb. 2005.
- [59] B. Han, J. Cheng, S. Li, G. Zhai, and J. Gao, "An improved small-signal model for SiGe HBTs," *International Journal of Electronics*, vol. 98, no. 6, pp. 781–791, Jun. 2011.
- [60] T. K. Johansen, J. Vidkjaer, and V. Krozer, "Substrate Effects in SiGe HBT Modeling," in *Proceedings of the 11th GAAS Symposium*, 2003, pp. 445–448.
- [61] U. Basaran, N. Wieser, G. Feiler, and M. Berroth, "Small-Signal and High-Frequency Noise Modeling of SiGe HBTs," *IEEE Transactions on Microwave Theory and Techniques*, vol. 53, no. 3, pp. 919–928, 2005.
- [62] A. Chakravorty, R. Garg, and C. K. Maiti, "Comparison of State-of-the-art Bipolar Compact Models for SiGe-HBTs," *Applied Surface Science*, vol. 224, pp. 354–360, 2004.
- [63] B. Heinemann, R. Barth, D. Bolze, J. Drews, P. Formanek, T. Grabolla, U. Haak, W. Hoppner, D. Knoll, K. Kopke, B. Kuck, R. Kurps, S. Marschmeyer, H. H. Richter, H. Rücker, P. Schley, and D. Schmidt, "Low-Parasitic Collector Construction for High-speed SiGe:C HBTs," in *International Electron Device Meeting*, 2004, pp. 251–254.
- [64] J. M. Rollett, "Stability and Power-Gain Invariants of Linear Twoports," *IRE Transactions on Circuit Theory*, vol. 9, no. 1, pp. 29–32, 1962.